NASA TM X-505

NASA TM X-505

2

TECHNICAL MEMORANDUM

X-505

FREE-FLIGHT MEASUREMENTS UP TO A MACH NUMBER OF 11 OF PRESSURE AND TURBULENT HEAT TRANSFER ON A BLUNTED CONE-CYLINDER WITH FLARED AFTERBODY

By Mamoru Inouye and Carr B. Neel

Ames Research Center
Moffett Field, Calif.

NATIONAL AERONAUTICS AND SPACE ADMINISTRATION

WASHINGTON

March 1961

NATIONAL AERONAUTICS AND SPACE ADMINISTRATION

TECHNICAL MEMORANDUM X-505

FREE-FLIGHT MEASUREMENTS UP TO A MACH NUMBER OF 11 OF PRESSURE AND TURBULENT HEAT TRANSFER ON A BLUNTED CONE-CYLINDER WITH FLARED AFTERBODY*

By Mamoru Inouye and Carr B. Neel

SUMMARY

A flight test was conducted with a blunted cone-cylinder model with flared afterbody. Results were obtained for Mach numbers from 9 to 11 and corresponding free-stream Reynolds numbers based on cylinder diameter from 2.6×10^6 to 3.7×10^6. Pressure measurements showed reasonable agreement with the machine computations of the flow field based on the method of characteristics. Measurements of the turbulent heat transfer showed good agreement with the Vaglio-Laurin theory.

INTRODUCTION

For missiles and other vehicles passing through the lower atmosphere at hypersonic speeds, the boundary layer may be almost entirely turbulent. Knowledge of the heating rates under these conditions is needed by the designer. Experimental investigations of turbulent boundary layers have been conducted in wind tunnels and shock tubes, but the extrapolation of these results to flight conditions is questionable because of the differences in Mach number, Reynolds number, and/or surface-temperature level that occur between the test conditions in ground facilities and in actual flight. Theoretical investigations of turbulent boundary layers rely on constants determined from these experiments, and the application of such semiempirical theories to flight conditions is similarly questionable. Therefore, a need exists for turbulent-heat-transfer data for conditions approaching those of actual flight, particularly on the cylindrical and flared afterbodies of blunt-nosed shapes.

Knowledge of the surface pressure and the flow properties at the outer edge of the boundary layer is a prerequisite for any analysis of the heat transfer to a body. Experimental data are required to define

*Title, Unclassified

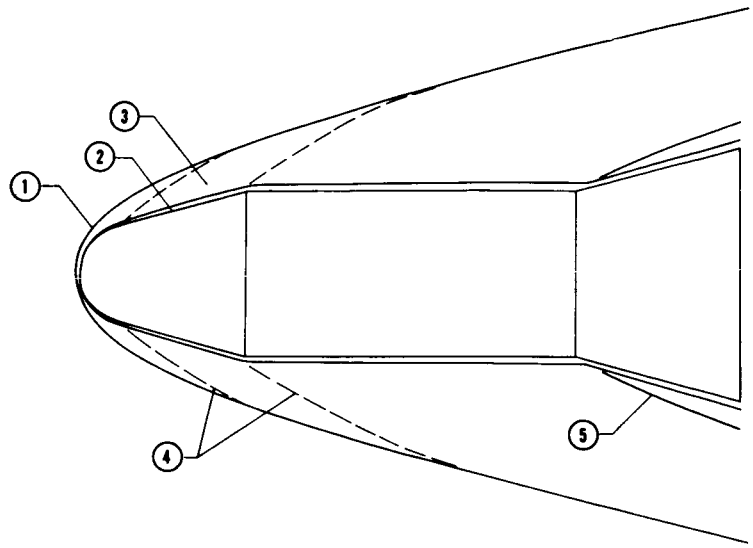

this flow field because for hypersonic flow over blunt bodies, the different flow regions and the interactions between them make it difficult to determine analytically the flow properties. The following sketch illustrates the flow field around the body of revolution considered in the present investigation. The important flow regions identified in the sketch are as follows:

1. A strong, detached bow wave that is normal near the stagnation point, curved and diminishing in strength away from the stagnation point, and approaching asymptotically a Mach wave at a large distance from the body.

2. A thin boundary layer on the body where viscous effects predominate.

3. An essentially inviscid layer between the boundary layer and the shock wave.

4. Expansion waves emanating from outside corners.

5. Shock wave emanating from an inside corner.

The present investigation is concerned with the free-flight measurement of the pressure distribution and turbulent heat transfer over the blunted cone-cylinder with flared afterbody shown in the preceding sketch. The flight test was conducted with a five-stage rocket system developed by Pilotless Aircraft Research Division, Langley Research Center, and launched from Wallops Island Flight Station. Acknowledgments are due Mr. Charles B. Rumsey and Mrs. Dorothy B. Lee of Langley Research Center and Messrs. C. Dewey Havill and Joseph Smith, Jr., of Ames Research Center for their direction and assistance in the flight test program. Dr. J. R. Sellars and Dr. H. Wohlwill of Space Technology Laboratories calculated the pressure distribution for the present model and flight conditions and made the results available for use in this report.

SYMBOLS

c	speed of sound, ft/sec
c_p	specific heat at constant pressure, Btu/lb $^{\circ}F$
D	cylinder diameter, ft
h	static enthalpy, Btu/lb
k	thermal conductivity, Btu/(sec ft^2 $^{\circ}F$/ft)
M	Mach number
Nu	Nusselt number, $\frac{q_w c_{p_s} s}{k_s(h_s-h_w)}$
p	static pressure, lb/ft^2
q	heat-transfer rate per unit area, Btu/sec ft^2
Re_∞	Reynolds number based on free-stream conditions, $\frac{\rho_\infty V_\infty D}{\mu_\infty}$
Re_s	Reynolds number based on stagnation point conditions, $\frac{s}{\mu_s}\sqrt{\rho_s p_s}$
s	distance along surface measured from stagnation point, feet unless indicated otherwise
t	time, sec
T	temperature, $^{\circ}F$
V	velocity, ft/sec
x, r	cylindrical coordinates of body surface, feet unless indicated otherwise
y	altitude, ft
α	angle of attack, deg
ρ	density, lb sec^2/ft^4
μ	viscosity, lb sec/ft^2

Subscripts

e	outer edge of boundary layer
n	thermocouple station number
r	reference condition
s	stagnation point on model
w	wall
∞	free stream

TEST EQUIPMENT

Model

The blunted cone-cylinder model with flared afterbody is shown in figures 1 and 2. For the purpose of obtaining transient-heat-transfer data with an isothermal surface, the wall thickness of the model was varied to reflect the calculated heating rate over the surface, so that the entire skin would heat uniformly. Wall thickness at the thermocouple stations is tabulated in figure 1. The skin was made of oxygen-free high-conductivity copper to minimize the thermal gradients perpendicular to the surface. No attempt was made to obtain a high quality surface finish - shop grade finish of 32 rms microinches was specified. A number of scratches and indentations were made in the soft copper shell during instrumentation and final assembly, but none were considered serious enough to disturb significantly either the pressure or temperature measurements.

To insure a turbulent boundary layer over the model, three-dimensional roughness was applied with a hand punch to the spherical nose ahead of the sonic point, where the roughness would not produce shock waves to disturb the flow downstream. The roughness was distributed in five concentric rings, each with 36 punch marks as shown in figure 3(a). Figure 3(b) is a close-up photograph of the punch marks. Each punch mark consisted of a depression with a peak at one end formed by the upsetting of the surface material. The average peak height, measured relative to the undisturbed surface, was 0.005 inch, which was approximately the calculated laminar boundary-layer thickness. Tests of small-scale models in the Ames supersonic free-flight range, under approximately the same conditions as would be experienced in flight, indicated that this roughness was sufficient to insure a turbulent boundary layer.

Instrumentation

Model instrumentation consisted of 3 accelerometers, 6 pressure cells, and 12 thermocouples. Data from these sources were transmitted over 10 telemetry channels with the accelerations and pressures being transmitted continuously over 9 separate channels and the temperatures being commutated and transmitted over the tenth channel.

The three accelerometers were located near the cylinder-flare juncture to measure the longitudinal and two lateral (tangential and normal) accelerations of the model. The range and accuracy of the accelerometers were as follows:

Accelerometer	Range, g	Accuracy, g
Longitudinal	-56 to +167	±3
Tangential	-20 to +20	±0.4
Normal	-20 to +20	±0.4

The six pressure cells were used to measure the stagnation point pressure, impact pressure at the outer edge of the boundary layer, and four static pressures along a meridian at the locations shown in figure 1. To withstand the aerodynamic heating, the stagnation point orifice and impact probe were machined from graphite. The former was a plug inserted in a hole drilled in the skin at the stagnation point, as shown in figure 1. The range and accuracy of the pressure measurements were as follows:

Pressure	Range, psia	Accuracy, psi
Stagnation point	0 to 235	±5
Cylinder impact	0 to 28	±0.6
Cone static	0 to 25	±0.5
Cylinder static (2)	0 to 14.7	±0.3
Flare static	0 to 14.7	±0.3

Twelve chromel-alumel thermocouples were installed on a meridian diametrically opposite the line of pressure orifices. Each thermocouple consisted of a pair of 30 gage wires with balled ends staked into place in holes drilled 0.040 inch deep and 0.10 inch apart in the inner surface, as indicated in figure 1. The junctions were thus formed at the inner surface. The thermocouple readings together with three reference voltages were sampled approximately six times per second. The zero, half, and full-scale temperatures corresponding to the reference voltages were 90° F, 960° F, and 1790° F for the cylinder stations, and 60° F, 930° F, and 1760° F for the cone and flare stations. The accuracy of the temperature data was approximately ±15° F.

TEST PROCEDURE

Model Trajectory

The model was boosted with a five-stage rocket system developed by Pilotless Aircraft Research Division, Langley Research Center. The model and boosters ready for launching at an elevation angle of 69° are shown in figure 4. Results of two of the previous tests performed with similar rockets are presented in references 1 and 2, which also describe the rocket system and test procedure. The latter reference includes the characteristics of the rocket motors.

The model trajectory is shown in figure 5. The motors of the first two stages, an Honest John and a Nike, were employed to boost the model and the last three stages to 87,000 feet. After a coast period, the motors of the last three stages, a Nike, Recruit, and T-55, were fired in succession during entry to obtain peak Mach and Reynolds numbers near fifth-stage or T-55 burnout. Failure of either the model or the fifth-stage motor at ignition resulted in loss of telemetry at a Mach number of 11. The variations of altitude, velocity, Mach number, and free-stream Reynolds number based on cylinder diameter during fourth-stage burning are shown in figure 6.

The model trajectory was determined in the following manner. Until third-stage ignition ($t = 103.2$ sec), the model position was obtained with the NASA modified SCR - 584 tracking radar. The model velocity was obtained with CW Doppler radar up to 30 seconds after launch and by differentiation of the tracking radar data from 30 seconds until third-stage ignition. After third-stage ignition, the model position and velocity were obtained by integrating the telemetered longitudinal accelerations of the model shown in figure 7. Lateral accelerations were found to have negligible effect on the trajectory. Atmospheric conditions up to an altitude of 70,000 feet were obtained four hours prior to model launch with a Rawinsonde carried aloft by a balloon and tracked by radar. The free-stream conditions of pressure, density, temperature, and speed of sound are shown in figure 8.

Reduction of Heat-Transfer Data

Appreciable heating of the model surface occurred only after fourth-stage ignition ($t \geq 106.8$ sec). The inside surface temperatures measured at the 12 thermocouple stations are plotted in figure 9. Data received after fifth-stage ignition ($t \geq 109.1$ sec) were disregarded because of the high angles of attack indicated by the surface pressures and lateral accelerations. Smooth curves were faired through the data points, and then Hill's numerical method (ref. 3) was used to calculate the outside

surface temperatures, also shown in figure 9, and the heat-transfer rates shown in figure 10. The temperature difference across the cylinder wall was only a few degrees, and hence the outside surface temperatures are not shown for stations 5 through 9. With the exception of the region near the stagnation point, the model shell was thin, and as a result of the large external heating rates, the longitudinal conduction effects were estimated to be small and, hence, were neglected. Near the stagnation point, the wall was thick, and no attempt was made to estimate the conduction effects.

Accuracy of Data

On the basis of previous flight tests with the same rocket system and consideration of the method of trajectory determination, the possible errors are estimated to be ±0.5 in the peak Mach number and ±2,000 feet in the corresponding altitude. The pressure measurements are accurate to ±2 percent of the full-scale value as tabulated in the Test Equipment section. The temperature measurements are believed accurate to ±15° F. The heat-transfer results are estimated to be accurate to ±15 percent during the latter portion of fourth-stage burning.

RESULTS AND DISCUSSION

Pressure

The ratio of measured stagnation point pressure to free-stream static pressure during fourth-stage burning is shown as a function of Mach number in figure 11. The sudden longitudinal acceleration of the model at fourth-stage ignition was probably responsible for the initial lag in the measured stagnation point pressure. In general, good agreement is obtained with both ideal- and real-gas theoretical values. Ideal-gas values were obtained from reference 4; real-gas values were computed using the method presented in reference 5 together with the thermodynamic properties of air presented in reference 6. The differences between the flight data and the theoretical values are within the experimental accuracy, the largest uncertainty being in the model altitude and hence free-stream static pressure.

The impact probe was intended to measure the impact pressure at the outer edge of the boundary layer on the cylinder and thus determine the flow properties in conjunction with the measured static pressure. However, because a low-range pressure cell was installed, no data were obtained for $M_\infty > 8$. Below a Mach number of 8, when the pressures were on-scale, the large fluctuations in angle of attack nullified the usefulness of the data.

The ratios of the measured surface pressures to the stagnation point pressure during fourth-stage burning are shown as functions of Mach number in figure 12. The pressure measured at the forward orifice on the cylinder was high compared to the aft cylinder pressure. Although the pressure at the forward location is expected to be high because of the proximity of the bow shock wave, it was from 50 to 100 percent higher than would be predicted from correlations based on experiments with similarly blunted models or predicted from theory. It is believed that the forward pressure orifice may have been disturbed by the impact probe, and consequently, its readings have been discounted. Appreciable fluctuations of the pressure occurred as a result of model pitching. However, dynamic stability of the fourth stage is indicated by the damping of the oscillations.

The measured cone pressure agrees well with modified Newtonian theory, as indicated by the comparison shown in figure 12. To estimate the angle of attack, the Newtonian pressures for $\pm 1^{\circ}$ angle of attack are also shown. It appears that for $M_{\infty} > 9$, the angle of attack in the plane of the pressure orifices was less than a degree. For $9 < M_{\infty} < 11$ the cone, cylinder, and flare pressures normalized by the stagnation point pressure are nearly independent of Mach number as expected for a blunt body in hypersonic flow. It should be noted that for this range of Mach numbers, the experimental accuracy was ±10 percent for the cone and flare pressure ratios and ±30 percent for the cylinder pressure ratio.

In figure 13 the measured pressures are compared with theoretical predictions for $M_{\infty} = 10$. Also shown are the limits of the flight data for $9 < M_{\infty} < 11$. As shown before in figure 12, modified Newtonian theory predicts the cone pressure very well. However, extension of the prediction of the flow field to the rest of the body by assuming a Prandtl-Meyer expansion from the cone to the cylinder and a compression through an oblique shock wave from the cylinder to the flare overestimates the pressures by a factor of two.

Because of the complexity of the flow over blunt bodies at hypersonic speed, probably the best theoretical predictions of the pressure distribution are based on machine calculations wherein real-gas thermodynamic properties are considered. A program for this type of calculation has been established by Space Technology Laboratories, Inc., and computations were performed for the test model at one flight condition. A brief outline of the machine computation program is as follows:

(1) The flow field between the detached shock wave and the hemispherical nose is calculated by the method of Garabedian and Lieberstein (ref. 7). Various shock shapes are assumed until the boundary condition that the nose shape be a spherical segment is satisfied.

(2) The flow field around the hemisphere, cone, and cylinder is calculated by the method of characteristics with the results of (1) being used as starting conditions.

(3) The flow field around the flared afterbody is calculated by the method of characteristics with the results from (2) being used for the conditions upstream of the flare shock wave.

The Space Technology Laboratories' calculations for the pressure distribution on the present model for flight conditions of $M_\infty = 10$ and $y = 64{,}000$ feet are shown in figure 13. Good agreement is obtained between the theoretical calculations and the flight data for the pressures on the cylinder and flare.

A 4. 4 2

Heat Transfer

The heat-transfer rate measured at thermocouple station number 1 near the stagnation point and normalized by dividing by the theoretical laminar value is shown as a function of Mach number in figure 14. For $M_\infty > 9$ the measured heat-transfer rates are 25 to 30 percent higher than theoretical laminar values which are the Fay and Riddell stagnation point values (ref. 8), multiplied by a factor of 0.96 given by Lees (ref. 9) for the reduction in heat transfer at a point 15° away from the stagnation point of a hemisphere. The theoretical turbulent sonic point heat-transfer rates given by Sibulkin (ref. 10) are about twice the theoretical laminar values. In view of the thick conductive wall at station number 1, it is reasonable that the indicated heat-transfer rate would be influenced by heating at both the stagnation point upstream from station number 1 and a possibly turbulent sonic point downstream from station number 1. It is believed that the high heat-transfer rate at station number 1 reflects this condition. Since this region of the model was not of primary interest in the investigation, no attempt was made to correct the data for conductive effects. The results are presented only for qualitative comparisons.

In figure 15 there are shown the turbulent heat-transfer rates measured at the 11 stations on the cone, cylinder, and flare and expressed in terms of $Nu/Re_s^{4/5}$, which is the correlating parameter for turbulent heat transfer used by Vaglio-Laurin in reference 11. The flight data are shown only for $M_\infty \geq 9$, for which the angle of attack was previously estimated to be less than a degree, and the heat-transfer rates were sufficiently large that the experimental error was ±15 percent or less. Since the method of data reduction, in which smooth curves were faired through a limited number of temperature data points (shown in fig. 9), tended to average the heat transfer over a range of Mach numbers, the results for $M_\infty = 9$ and 11 are shown only as limits of the results for $M_\infty = 10$. The deviations from the $M_\infty = 10$ results are within the experimental accuracy. The low heat transfer at the first cone station (number 2) was probably due to unestablished turbulent flow. The low heat transfer at the first cylinder station (number 5) might have been caused by a slight separation of the flow after the sharp cone-cylinder juncture.

Since the heat-transfer rates at the last cylinder station (number 9) and the first flare station (number 10) do not differ markedly from those at adjacent upstream and downstream stations, respectively, the flow was apparently attached at these stations. Hence, the extent of any separated region at the cylinder-flare juncture was small.

The flight-test results are compared in figure 15 with a number of turbulent-heat-transfer theories. Since the measured pressures were insufficient in number and accuracy to define a pressure distribution along the model as required for the heat-transfer theories, it was considered advisable to use the calculated pressure distribution in the heat-transfer predictions. In addition, the use of a theoretical pressure distribution offers a procedure for predicting the heat transfer to a body without initially measuring the pressures.

For any of the theories, the predicted heat-transfer rates for $M_\infty = 9$ or 11 differ by less than 5 percent from the heat-transfer rate for $M_\infty = 10$; thus, only the predictions for $M_\infty = 10$ are shown. Good agreement is obtained over the whole model with the Vaglio-Laurin theory (ref. 11) and the Cresci, MacKenzie, and Libby theory (ref. 12). The reference enthalpy method (ref. 13), the Rose, Adams, and Probstein theory (ref. 14), the Bromberg, Fox, and Ackerman theory (ref. 15), and the Van Driest theory (ref. 16) predict heat-transfer rates that are 10 to 40 percent higher than the Vaglio-Laurin theory and do not show as good agreement with the present flight data. If the calculated pressure distribution were adjusted to agree with the measured pressures, the corresponding Vaglio-Laurin heat-transfer prediction would still yield the best agreement with the flight data for the cone and flare. Only on the cylinder where the measured pressure was subject to ±30-percent error would the Vaglio-Laurin theory fail to give as good agreement with the flight data as the other theories.

The theoretical methods of Cresci, et al., Rose, et al., and Bromberg, et al., are quite similar. The momentum integral equation is solved by assuming the Blasius or a similar incompressible relationship for the skin-friction coefficient. Then the Reynolds analogy is used to obtain the heat transfer. The result is an essentially incompressible relationship for heat transfer with flow properties evaluated at the outer edge of the boundary layer. This relationship is modified by a factor which depends on the previous history of the flow at the outer edge of the boundary layer and which generally affects the heat transfer by less than 15 percent. The Van Driest theory and the reference enthalpy method were developed for a compressible turbulent boundary layer on a flat plate with zero pressure gradient. According to the Van Driest theory, the compressibility and surface temperature level effects counteract each other for the present case of flow at high free-stream Mach numbers over a cool blunt body, and the heat transfer is close to the incompressible value. In the reference enthalpy method an incompressible relationship for heat transfer is used with the compressibility and surface temperature

level effects being taken into consideration by evaluating the flow properties at the reference conditions defined by an empirical relation for the reference enthalpy. For the present flow conditions, the reference enthalpy is approximately equal to the enthalpy at the outer edge of the boundary layer. Hence, the theoretical predictions of references 13 to 16 yield approximately the same heat transfer.

The reason the Vaglio-Laurin and Cresci, et al., theories predict lower heat transfer rates than the others is that their skin-friction relationships are multiplied by a ratio of viscosities, μ_e/μ_r, where μ_r is the viscosity at some reference condition. This factor appears in the Vaglio-Laurin theory because he considered the compressibility effects by introducing a coordinate transformation which reduced the compressible turbulent boundary-layer equations to equivalent incompressible equations for flow at high free-stream Mach numbers over a cool blunt body. The resulting relationships express the compressible turbulent skin-friction coefficient as being directly proportional to an essentially incompressible value established from the transformed coordinates and with the constant of proportionality being equal to μ_e/μ_r. Vaglio-Laurin suggested the use of the stagnation point as the reference condition and was able to correlate wind-tunnel heat-transfer measurements with his theory in reference 11. Cresci, et al., followed Vaglio-Laurin's suggestion and modified their skin-friction coefficient accordingly. It is noteworthy that if the factor, μ_e/μ_s, is removed from the expressions of Vaglio-Laurin and Cresci, et al., their predictions for heat transfer would be approximately the same as the other theories. The present data appear to corroborate the Vaglio-Laurin theory, including the transformation of the boundary-layer equations and the suggestion that the stagnation conditions be used as the reference conditions, for a test conducted under actual flight conditions.

CONCLUSIONS

The following results were obtained from a flight test of a blunted cone-cylinder model with flared afterbody at Mach numbers up to 11 and free-stream Reynolds numbers based on the cylinder diameter up to 3.7×10^6.

Pressure measurements showed the stagnation point pressure to be in good agreement with ideal- and real-gas predictions. The cylinder and flare pressures were predicted better by the Space Technology Laboratories machine computations of the flow field using the method of characteristics than by modified Newtonian theory, combined with a Prandtl-Meyer expansion and an oblique shock compression. The cone pressure was predicted by modified Newtonian theory.

The heat-transfer results near the stagnation point and forward of the boundary-layer trip indicated a laminar boundary layer at that point. The heat-transfer results on the cone, cylinder, and flare indicated a turbulent boundary layer and showed good agreement with the Vaglio-Laurin theory used in conjunction with the calculated pressure distribution. Other available theories including the reference enthalpy method overestimated the heat-transfer rates.

Ames Research Center
National Aeronautics and Space Administration
Moffett Field, Calif., Dec. 14, 1960

REFERENCES

1. Rumsey, Charles B., and Lee, Dorothy B.: Heat-Transfer Measurements in Free Flight at Mach Numbers up to 14.6 on a Flat-Faced Conical Nose with a Total Angle of 29°. NACA RM L57L03, 1958.

2. Bland, William M., Jr., Swanson, Andrew G., and Kolenkiewicz, Ronald: Free-Flight Aerodynamic-Heating Data at Mach Numbers up to 10.9 on a Flat-Faced Cylinder. NACA RM L57K29, 1958.

3. Hill, P. R.: A Method of Computing the Transient Temperature of Thick Walls from Arbitrary Variation of Adiabatic-Wall Temperature and Heat-Transfer Coefficient. NACA Rep. 1372, 1958.

4. Ames Research Staff: Equations, Tables, and Charts for Compressible Flow. NACA Rep. 1135, 1953.

5. Moeckel, W. E.: Oblique-Shock Relations at Hypersonic Speeds for Air in Chemical Equilibrium. NACA TN 3895, 1957.

6. Moeckel, W. E., and Weston, Kenneth C.: Composition and Thermodynamic Properties of Air in Chemical Equilibrium. NACA TN 4265, 1958.

7. Garabedian, P. R., and Lieberstein, H. M.: On the Numerical Calculation of Detached Bow Shock Waves in Hypersonic Flow. Jour. Aero. Sci., vol. 25, no. 2, Feb. 1958, pp. 109-118.

8. Fay, J. A., and Riddell, F. R.: Theory of Stagnation Point Heat Transfer in Dissociated Air. Jour. Aero. Sci., vol. 25, no. 2, Feb. 1958, pp. 73-85.

9. Lees, Lester: Laminar Heat Transfer Over Blunt-Nosed Bodies at Hypersonic Flight Speeds. Jet Propulsion, vol. 26, no. 4, April 1956, pp. 259-269.

10. Sibulkin, Merwin: Estimation of Turbulent Heat Transfer at the Sonic Point of a Blunt-Nosed Body. Jet Propulsion, vol. 28, no. 8, part 1, Aug. 1958, pp. 548-554.

11. Vaglio-Laurin, Roberto: Turbulent Heat Transfer on Blunt-Nosed Bodies in Two-Dimensional and General Three-Dimensional Hypersonic Flow. Jour. Aero/Space Sci., vol. 27, no. 1, Jan. 1960, pp. 27-36.

12. Cresci, Robert J., MacKenzie, Donald A., and Libby, Paul A.: An Investigation of Laminar, Transitional, and Turbulent Heat Transfer on Blunt-Nosed Bodies in Hypersonic Flow. Jour. Aero/Space Sci., vol. 27, no. 6, June 1960, pp. 401-414.

13. Eckert, Ernst R. G.: Survey on Heat Transfer at High Speeds. WADC Tech. Rep. 54-70, April 1954.

14. Rose, Peter H., Adams, Mac C., and Probstein, Ronald F.: Turbulent Heat Transfer on Highly Cooled Blunt Nosed Bodies of Revolution in Dissociated Air. 1958 Heat Transfer and Fluid Mechanics Institute, Univ. of Calif., Berkeley, June 1958, pp. 143-155.

15. Anon.: Polaris Missile System, FTV 3 Series, Special Test Vehicles Missile Final Test Report, Lockheed Aircraft Corp., Missile Systems Division, Sunnyvale, Calif. LMSD-2733, Aug. 1958.

16. Lee, Dorothy B., and Faget, Maxime A.: Charts Adapted from Van Driest's Turbulent Flat-Plate Theory for Determining Values of Turbulent Aerodynamic Friction and Heat Transfer Coefficients. NACA TN 3811, 1956.

[redacted]

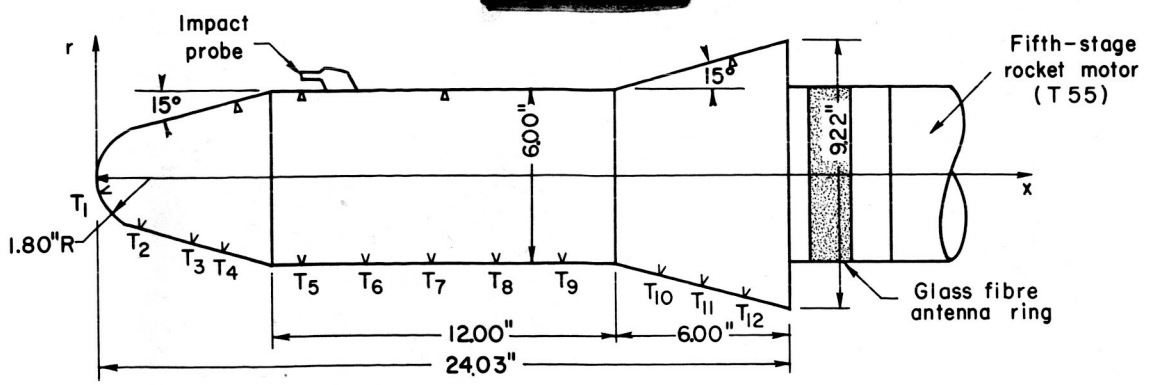

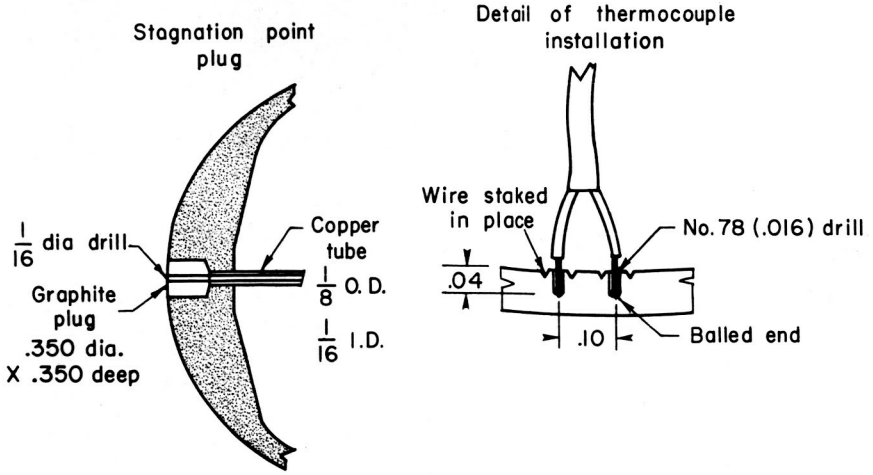

V THERMOCOUPLE STATIONS

n	x, in.	s, in.	s/D	Wall thickness, in.
1	0.06	0.47	0.078	0.590
2	1.38	2.43	.404	.181
3	3.25	4.36	.726	.184
4	4.40	5.55	.926	.185
5	6.97	8.18	1.364	.071
6	9.22	10.43	1.738	.073
7	11.47	12.68	2.114	.073
8	13.72	14.93	2.488	.073
9	15.97	17.18	2.864	.073
10	19.48	20.74	3.458	.120
11	20.92	22.24	3.708	.123
12	22.37	23.74	3.958	.132

Δ PRESSURE ORIFICES

Location	x, in.	s, in.	s/D
Stagnation point	0	0	0
Cone	4.77	5.94	.990
Cylinder	7.09	8.30	1.384
Impact probe	7.09	8.30	1.384
Cylinder	12.03	13.24	2.206
Flare	21.95	23.30	3.884

Figure 1.- Model configuration and instrumentation.

C[redacted]

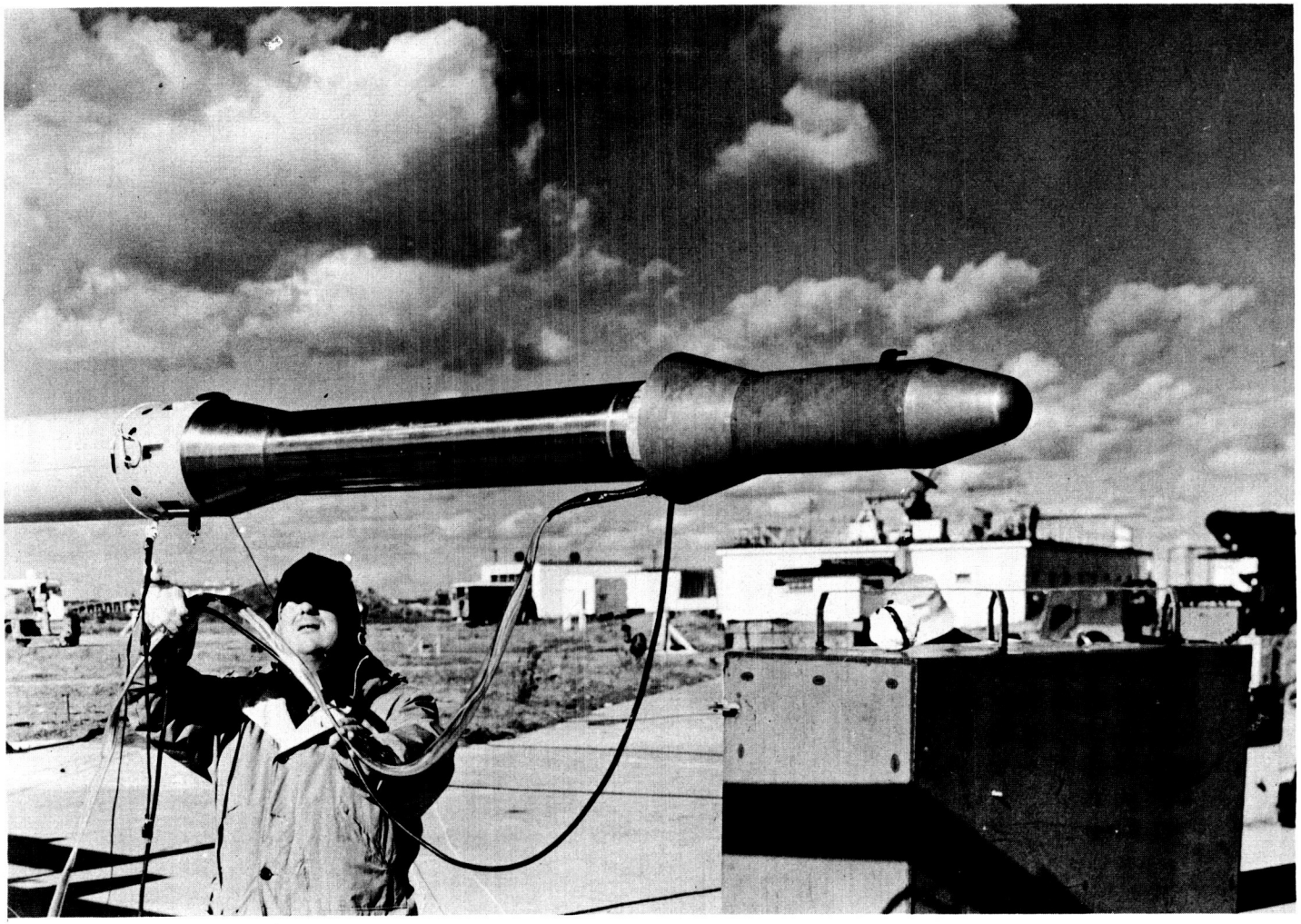

A-26133

Figure 2.- Model and fifth-stage rocket motor.

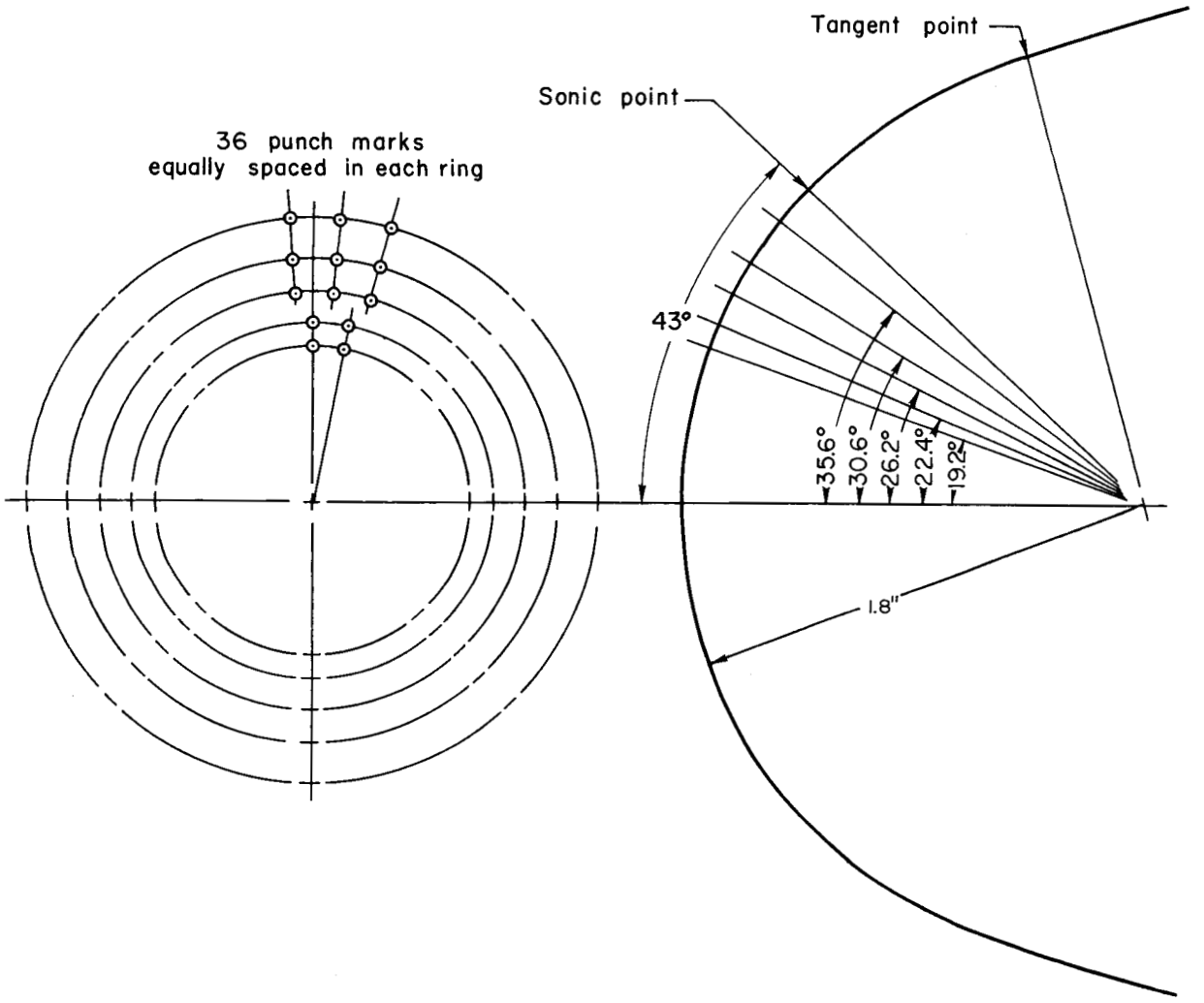

(a) Distribution of roughness.

Figure 3.- Boundary-layer trip on hemisphere.

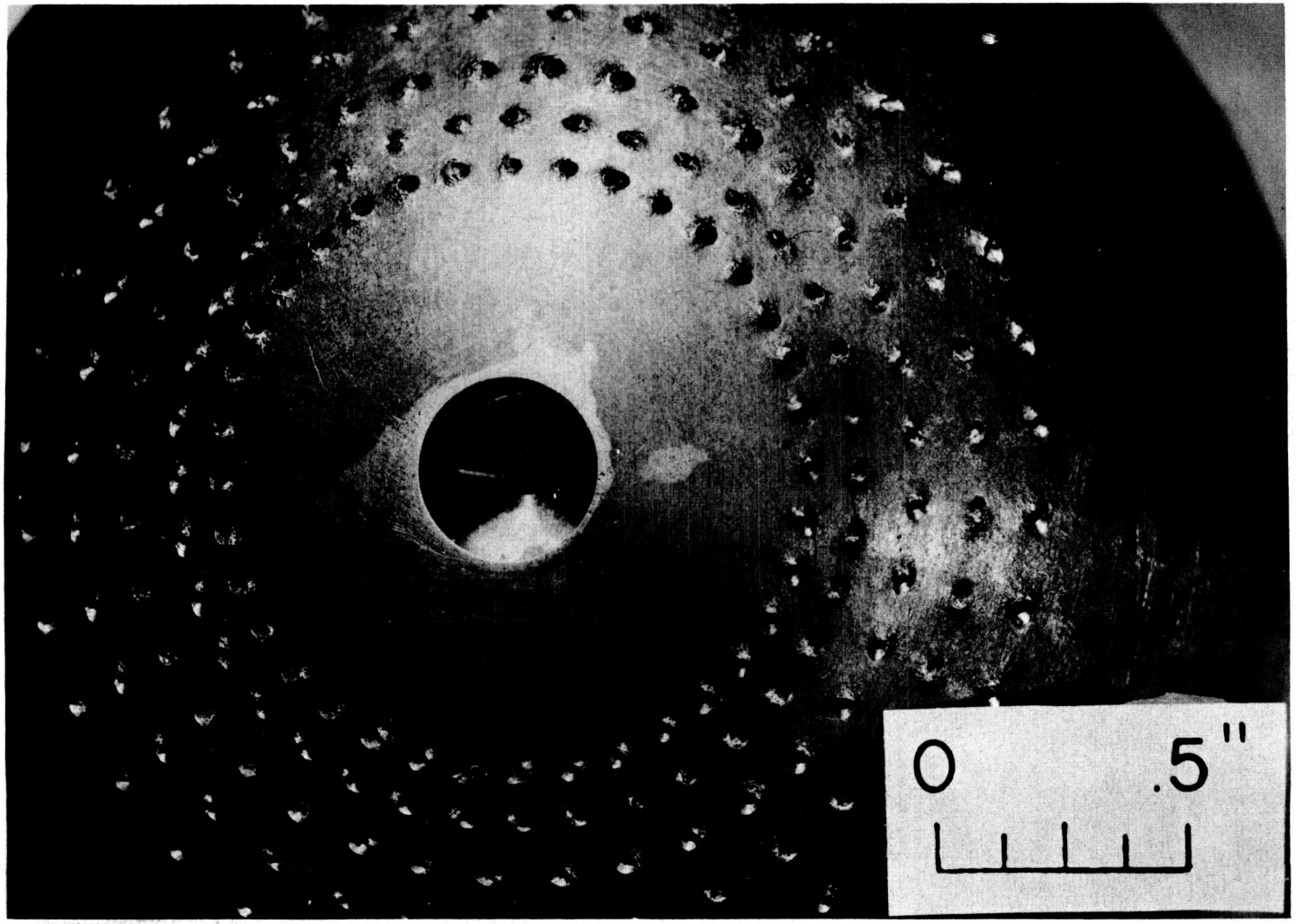

A-25329

(b) Close-up of roughness.

Figure 3.- Concluded.

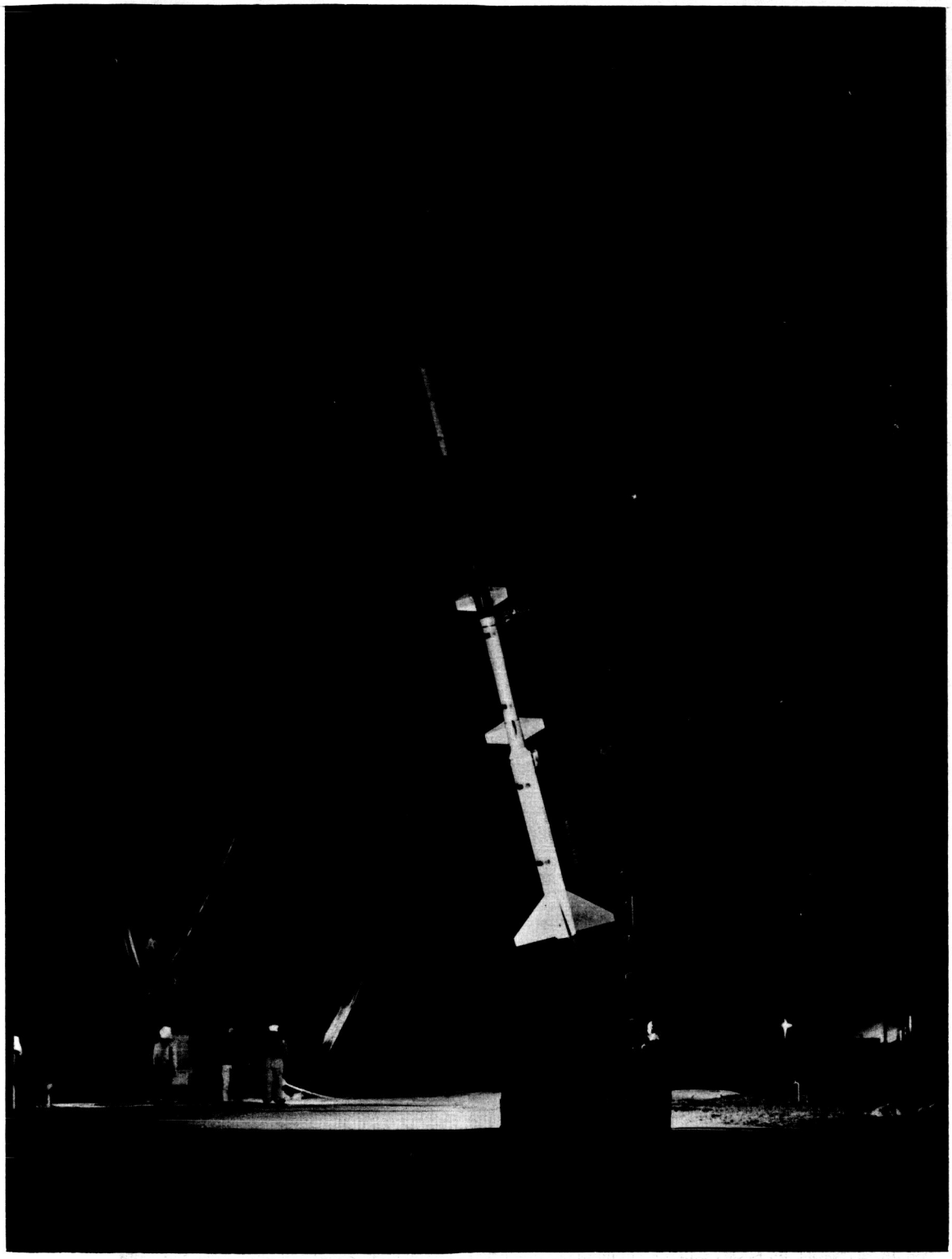

A-26131

Figure 4.- Five-stage rocket ready for launching.

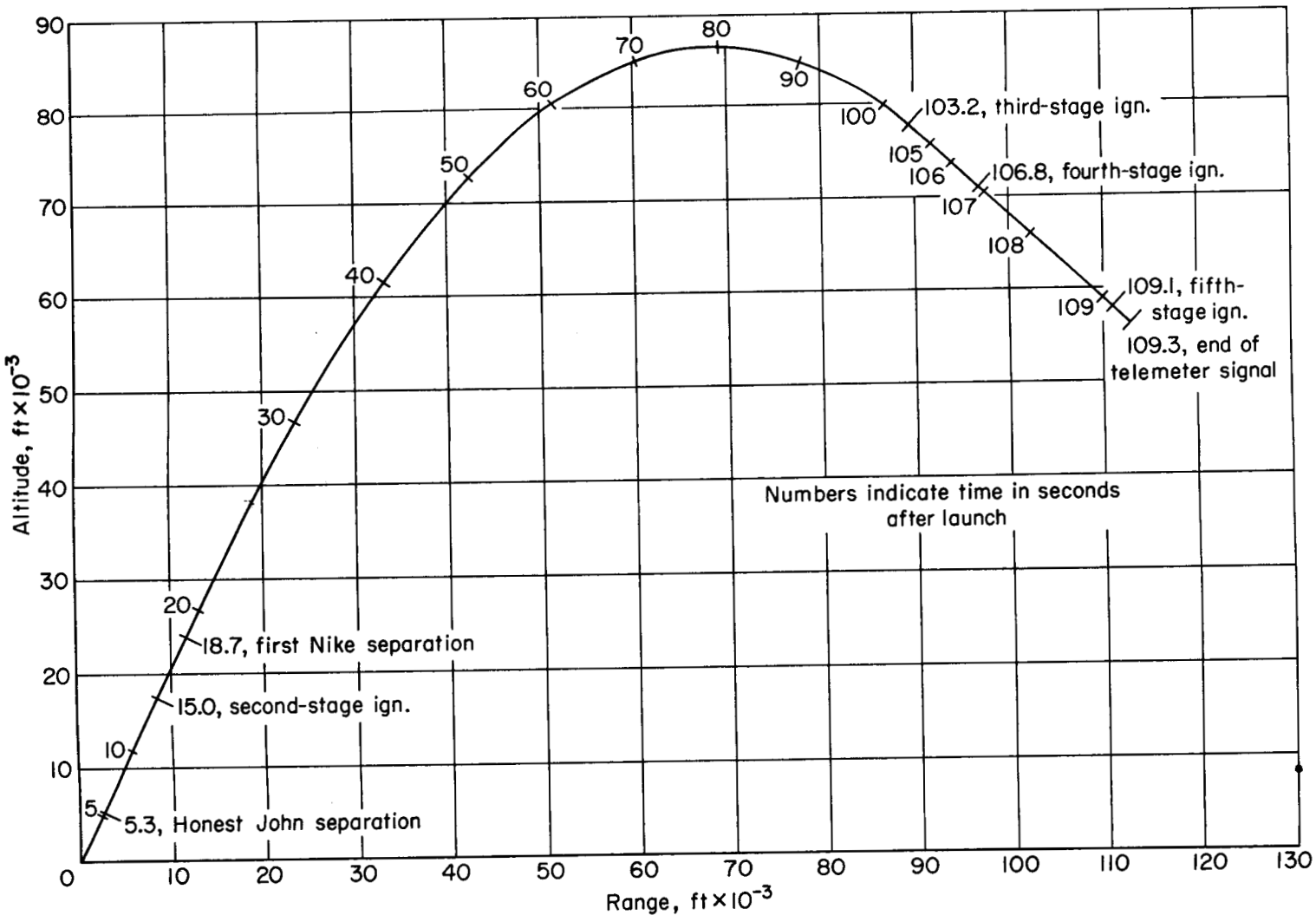

Figure 5.- Model trajectory.

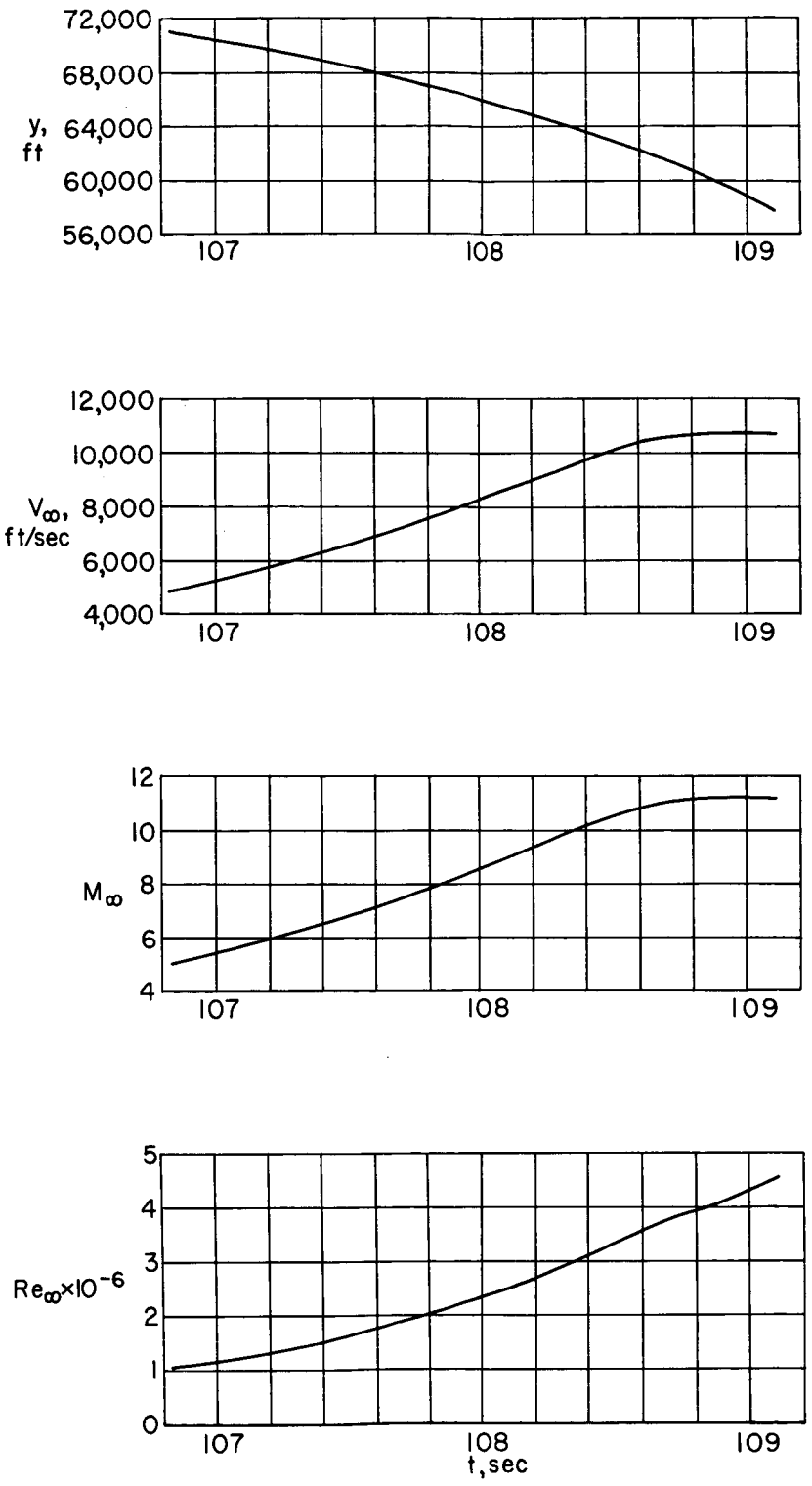

Figure 6.- Flight conditions during fourth-stage burning.

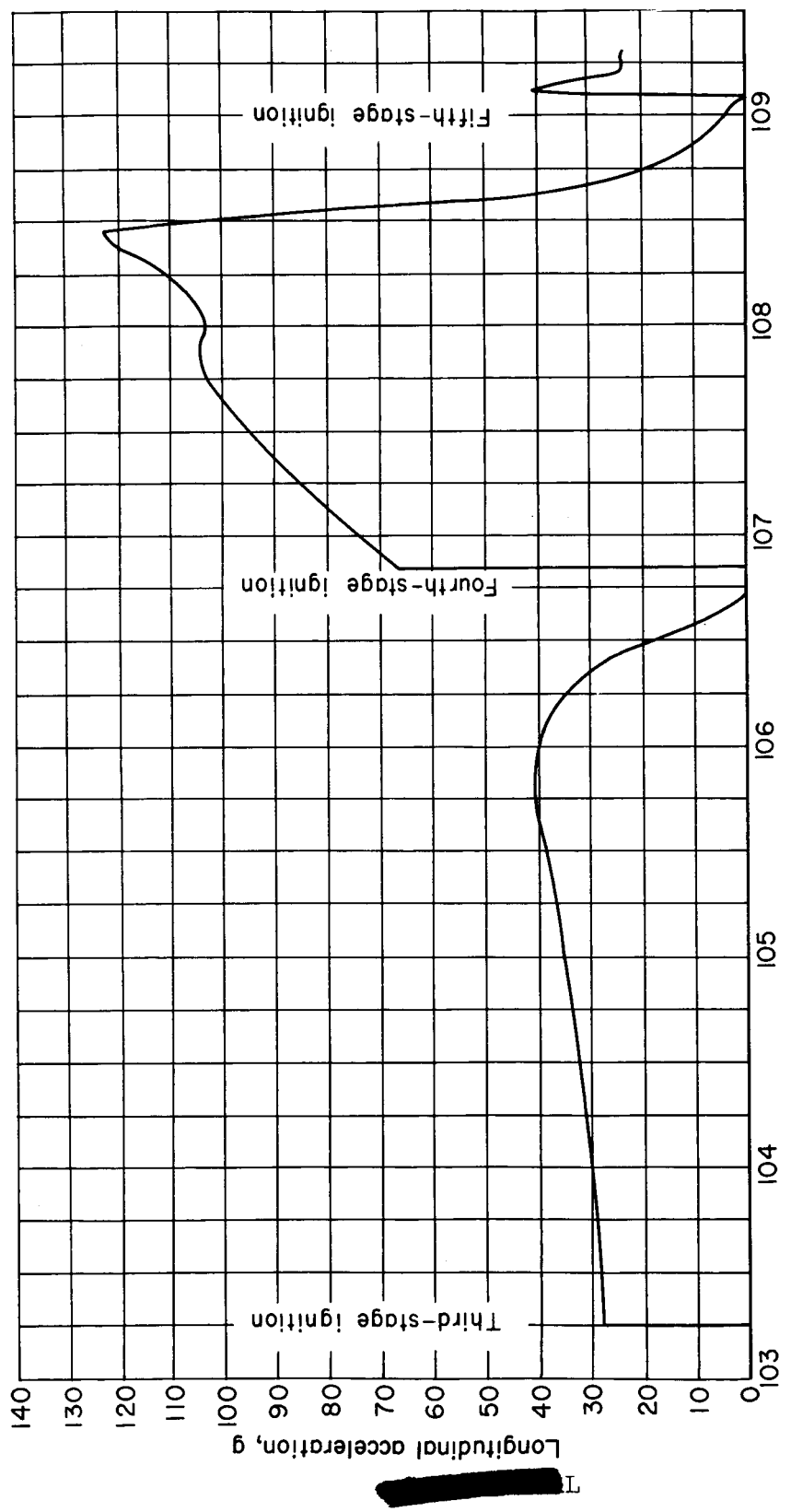

Figure 7.- Longitudinal acceleration after third-stage ignition.

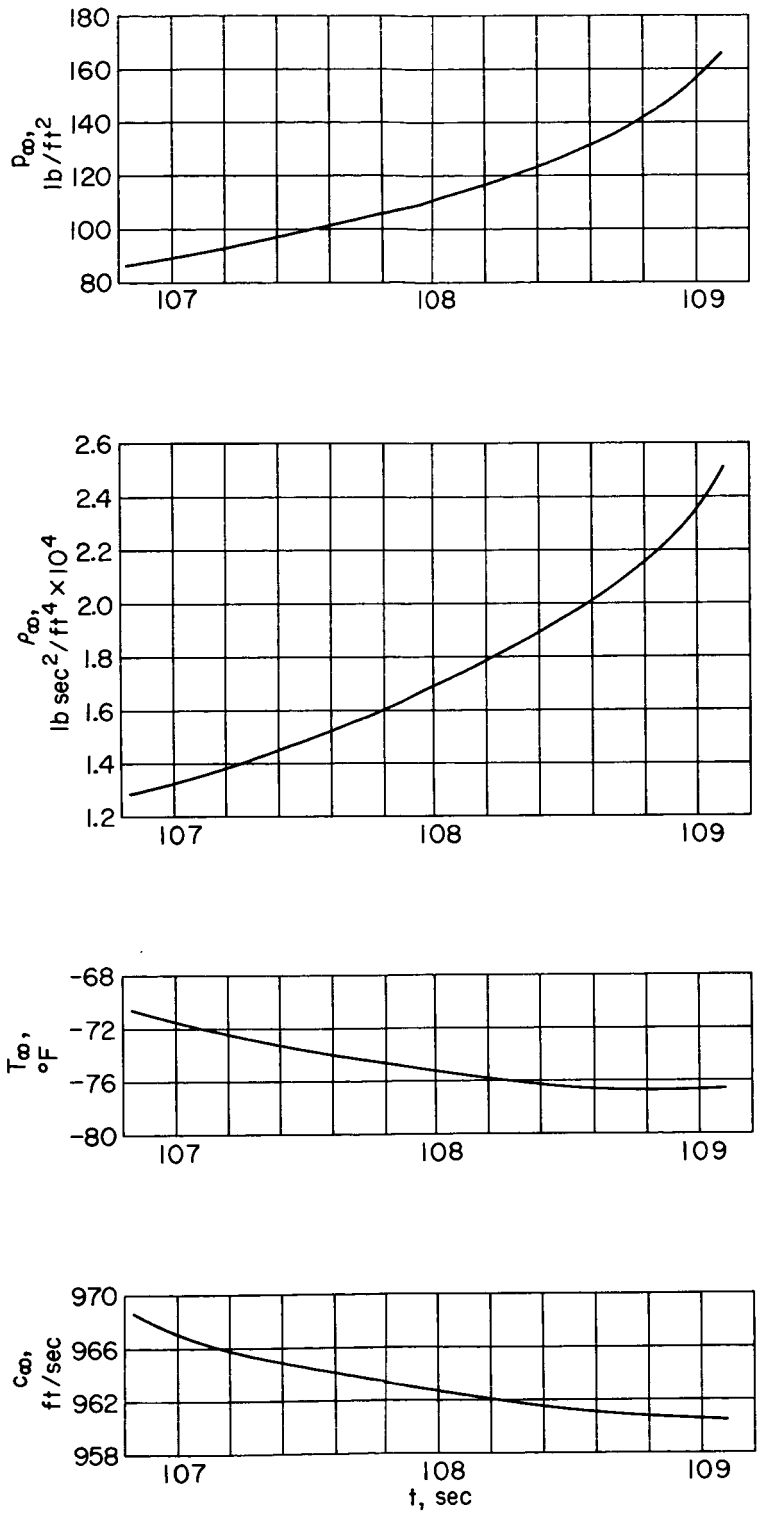

Figure 8.- Free-stream conditions during fourth-stage burning.

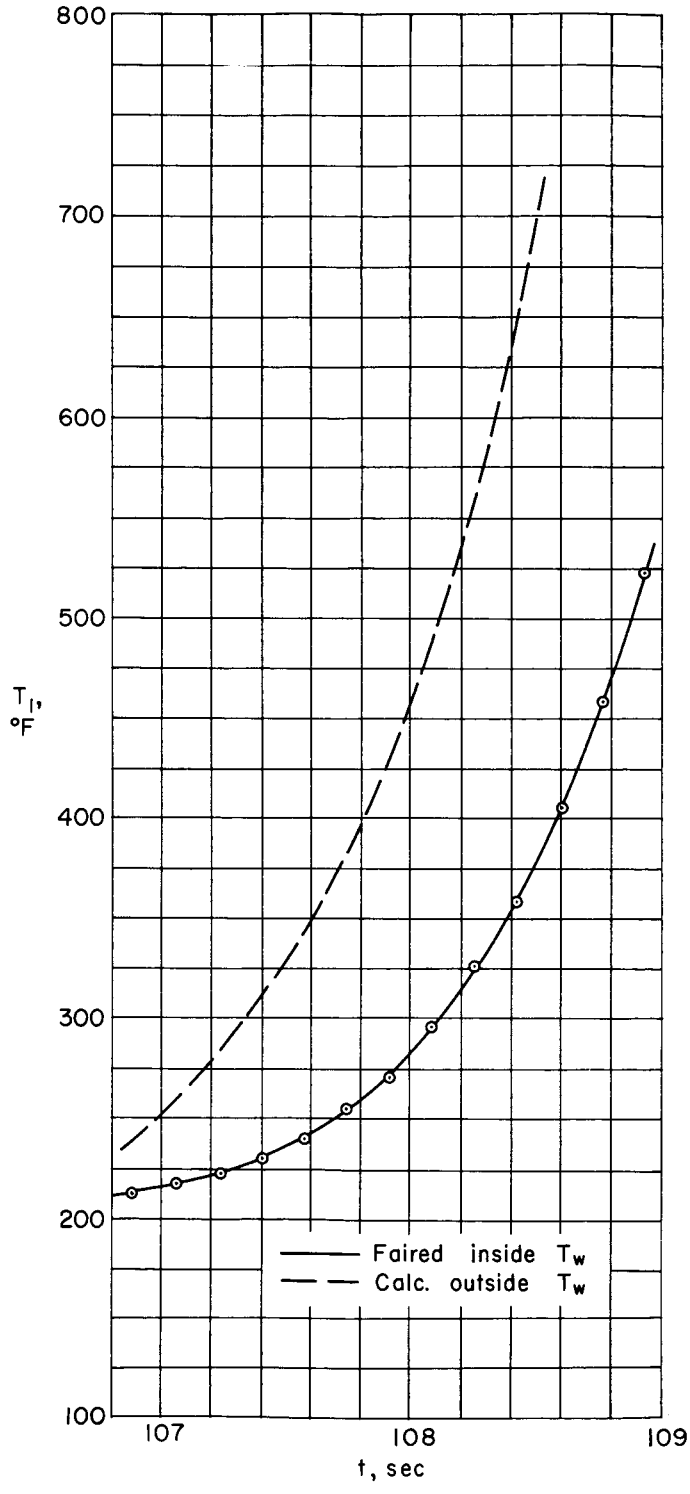

(a) Nose station.

Figure 9.- Wall temperature histories during fourth-stage burning.

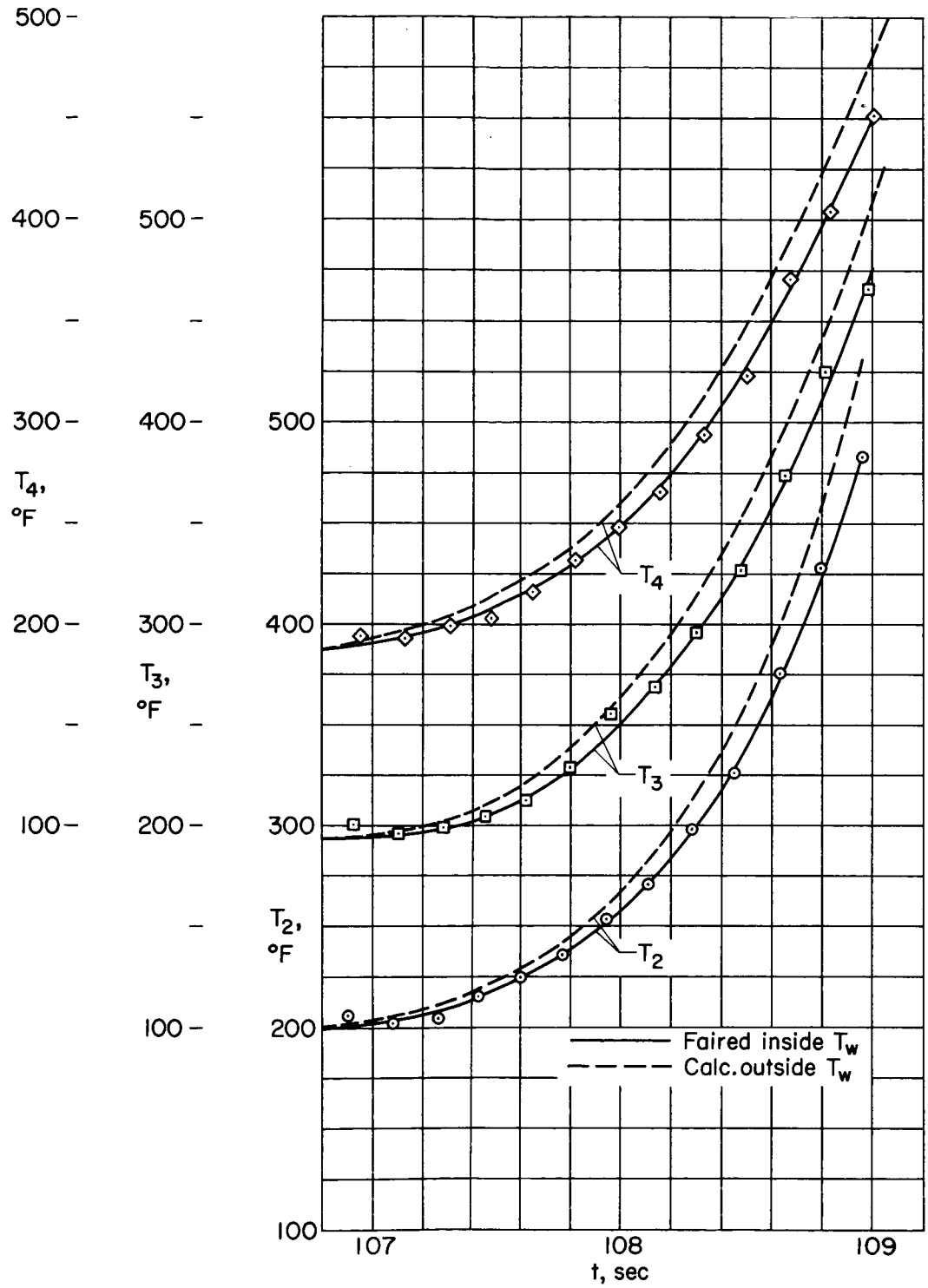

(b) Cone stations.

Figure 9.- Continued.

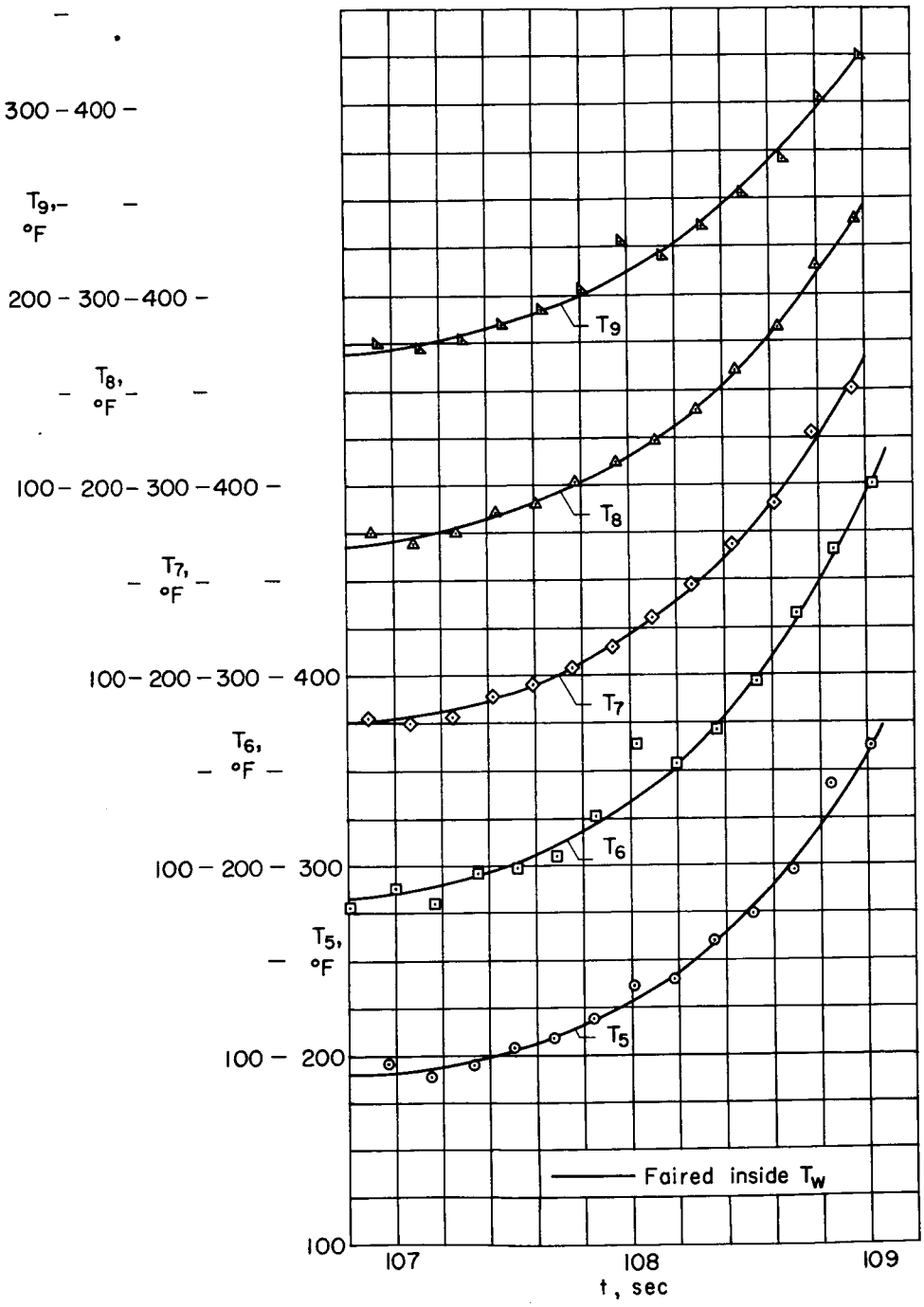

(c) Cylinder stations.

Figure 9.- Continued.

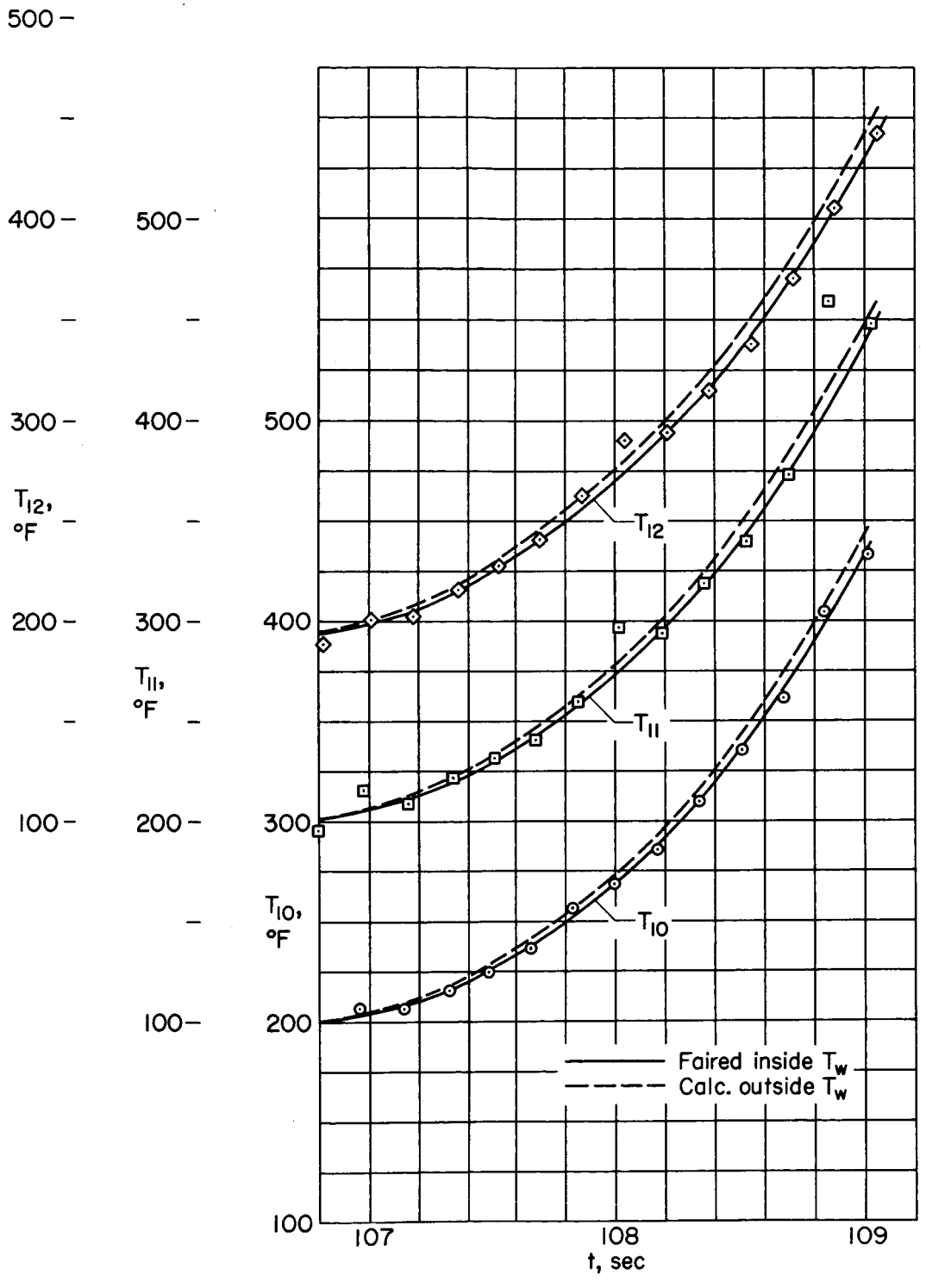

(d) Flare stations.

Figure 9.- Concluded.

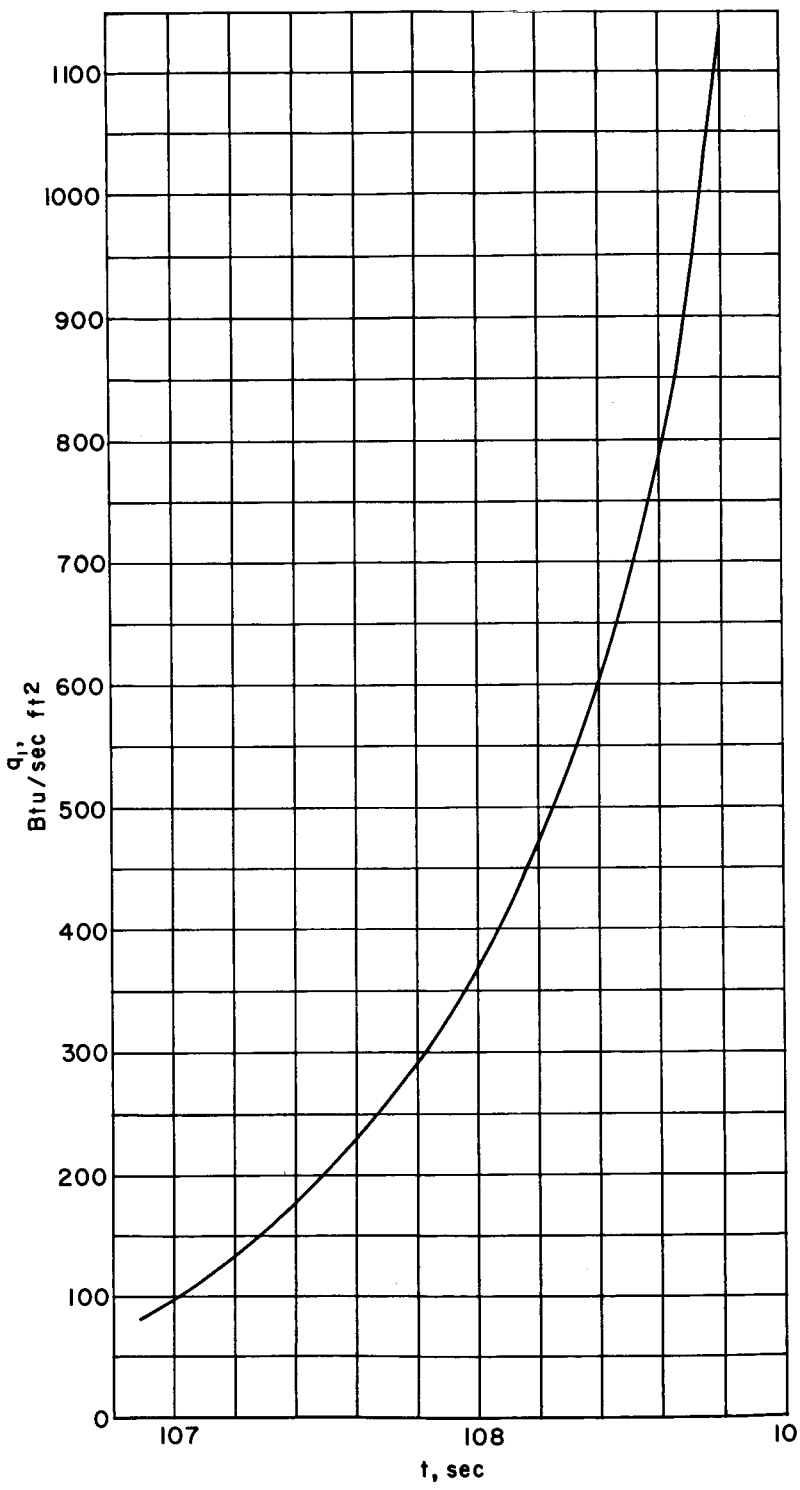

(a) Nose station.

Figure 10.- Heating rates during fourth-stage burning.

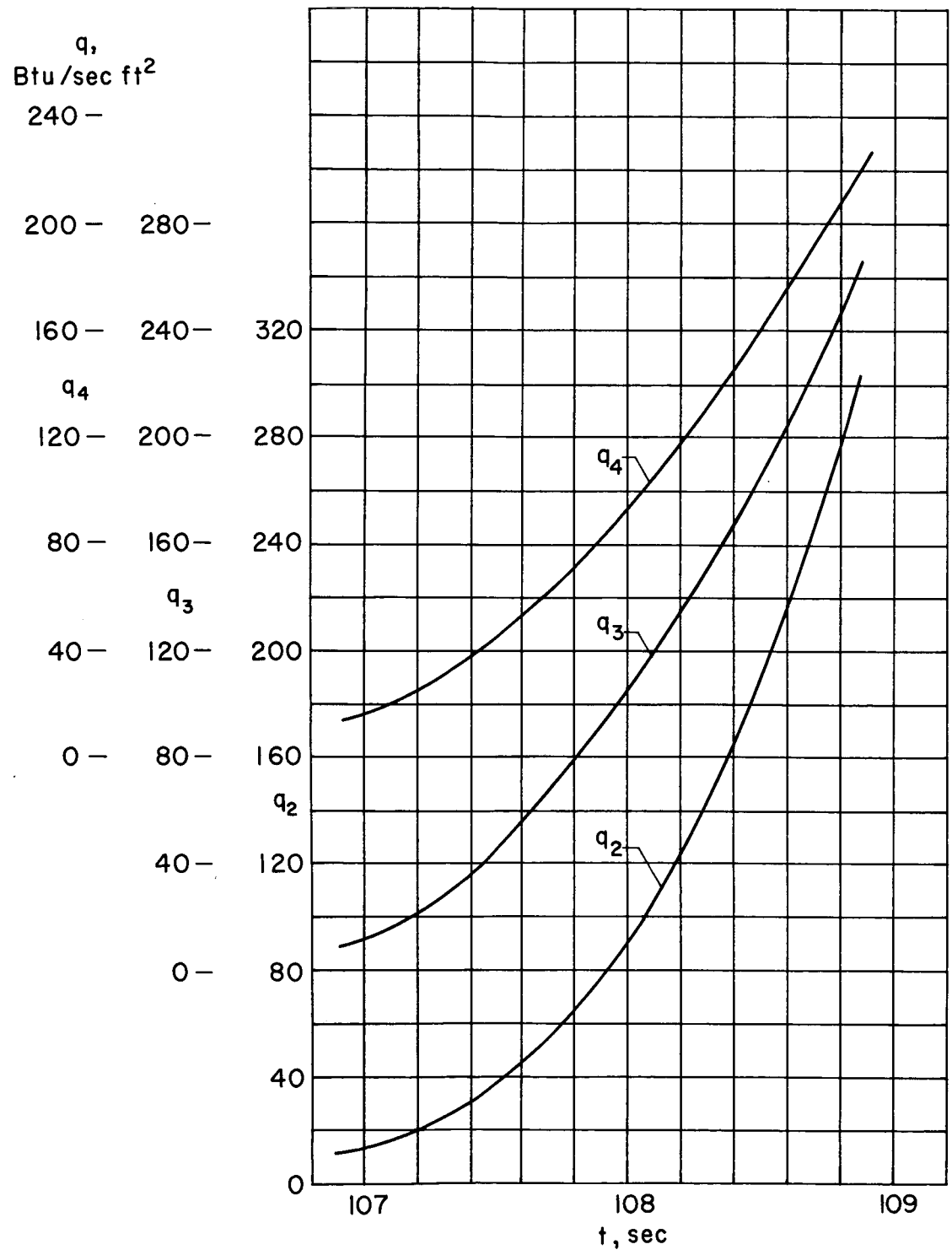

(b) Cone stations.

Figure 10.- Continued.

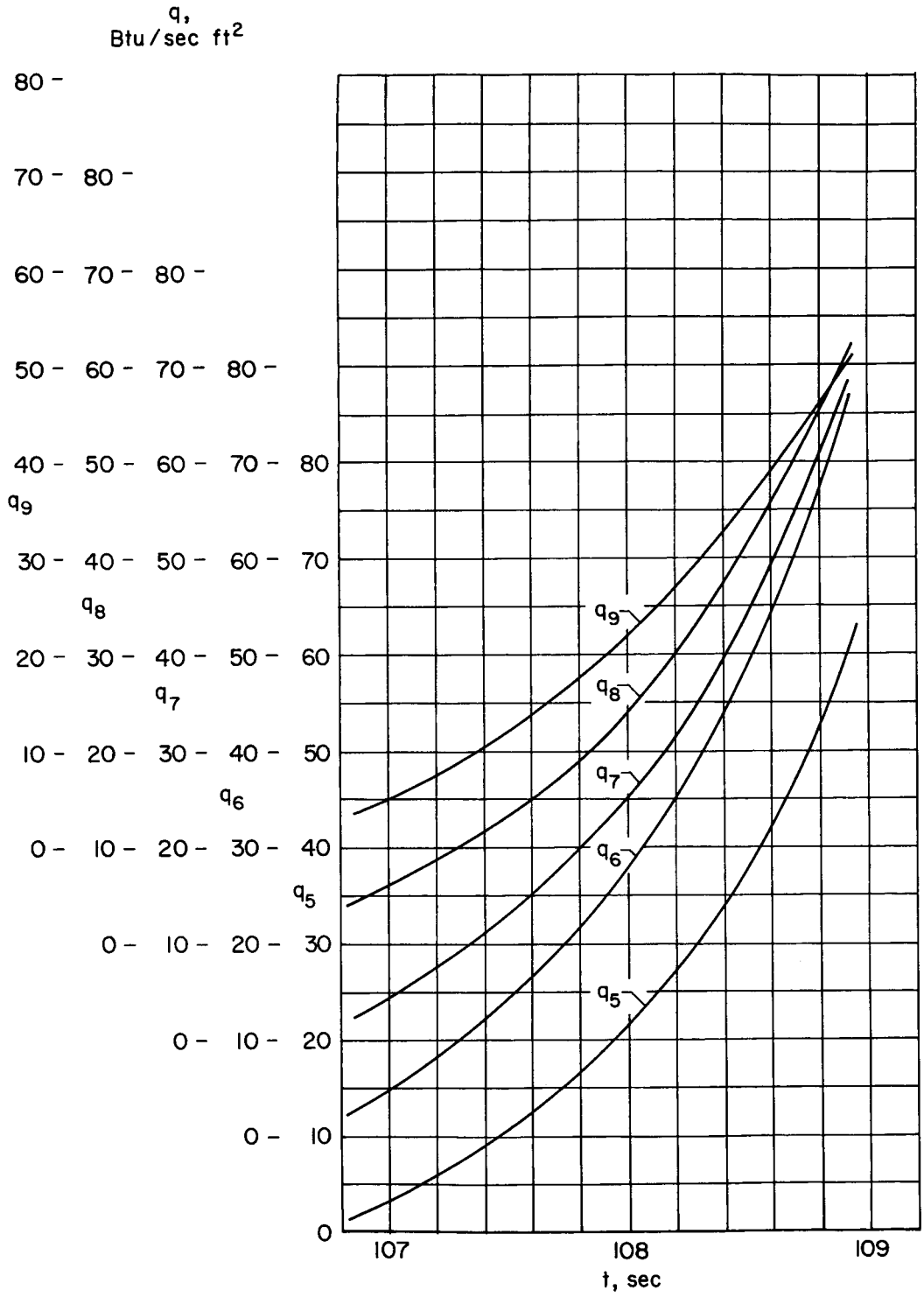

(c) Cylinder stations.

Figure 10.- Continued.

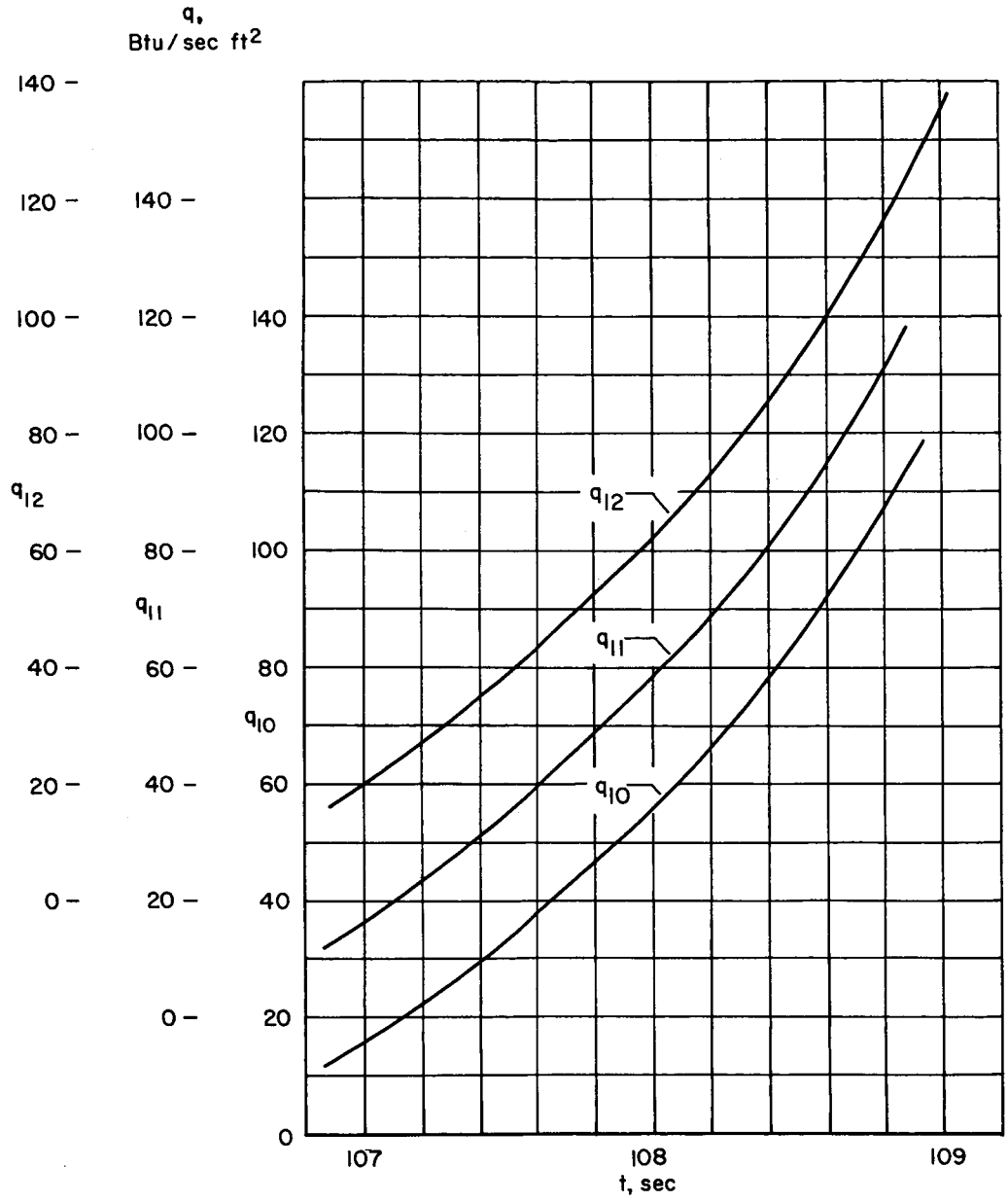

(d) Flare stations.

Figure 10.- Concluded.

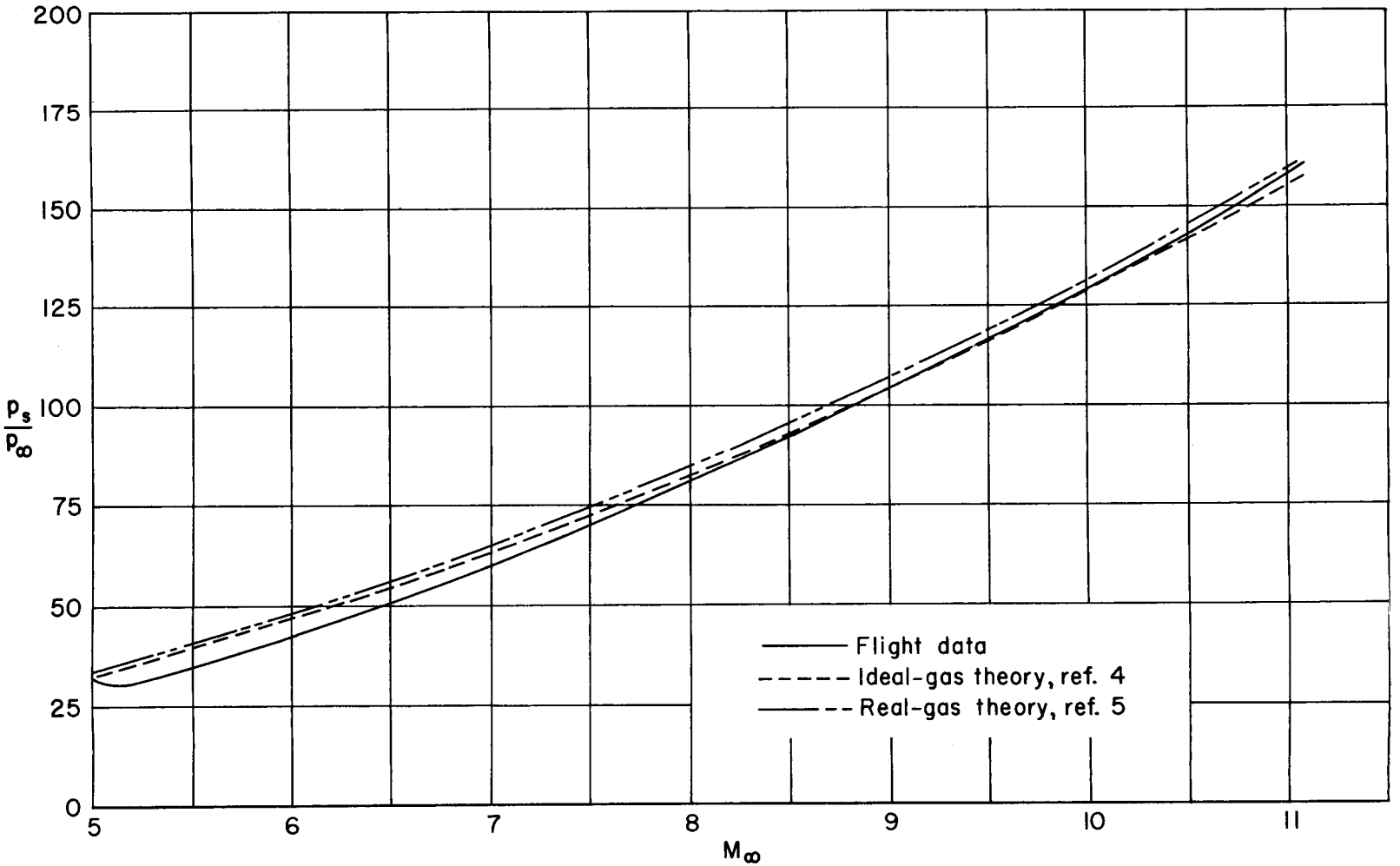

Figure 11.- Ratio of stagnation-point to free-stream static pressure as a function of Mach number during fourth-stage burning.

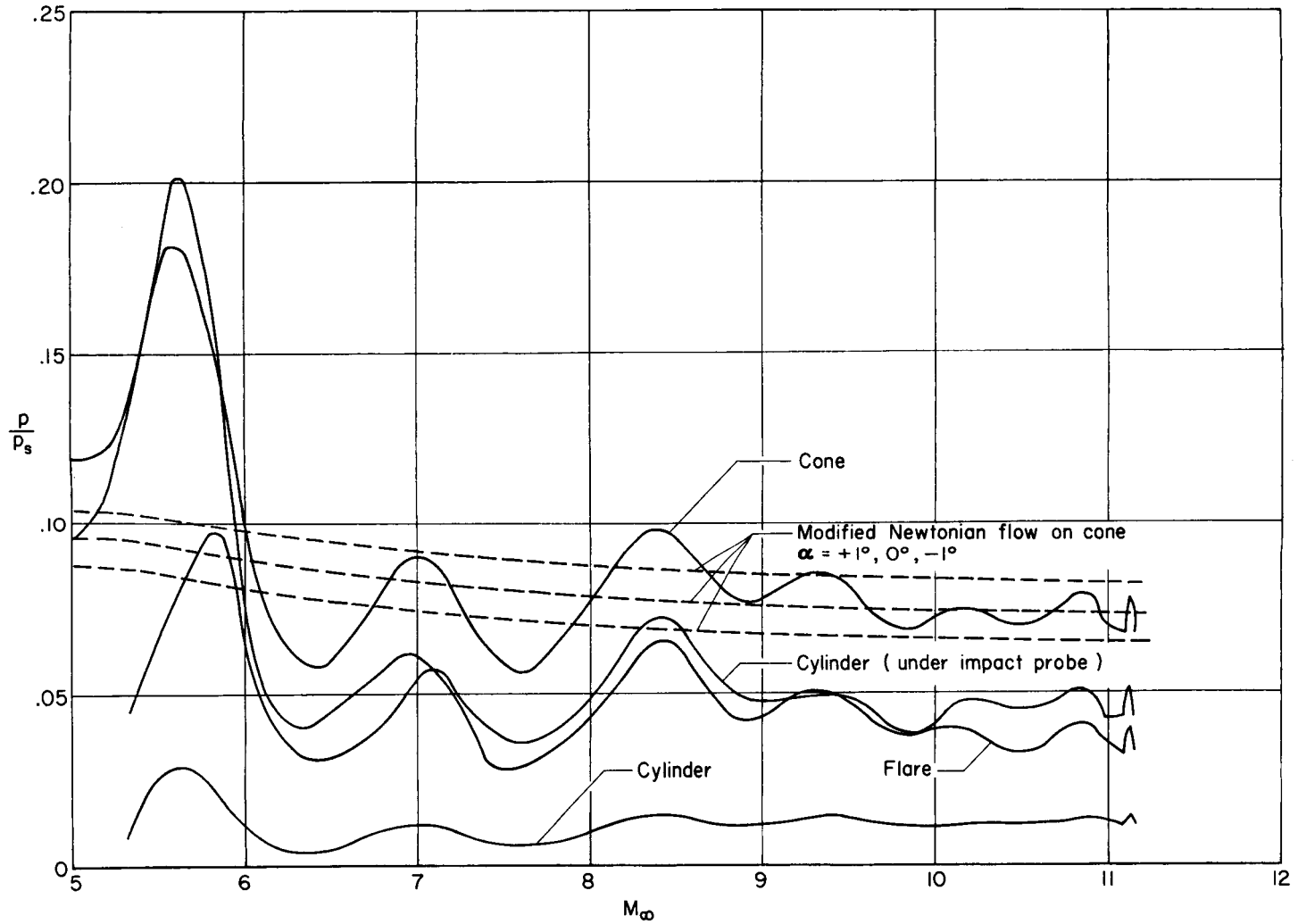

Figure 12.- Ratios of surface to stagnation-point pressure as functions of Mach number during fourth-stage burning.

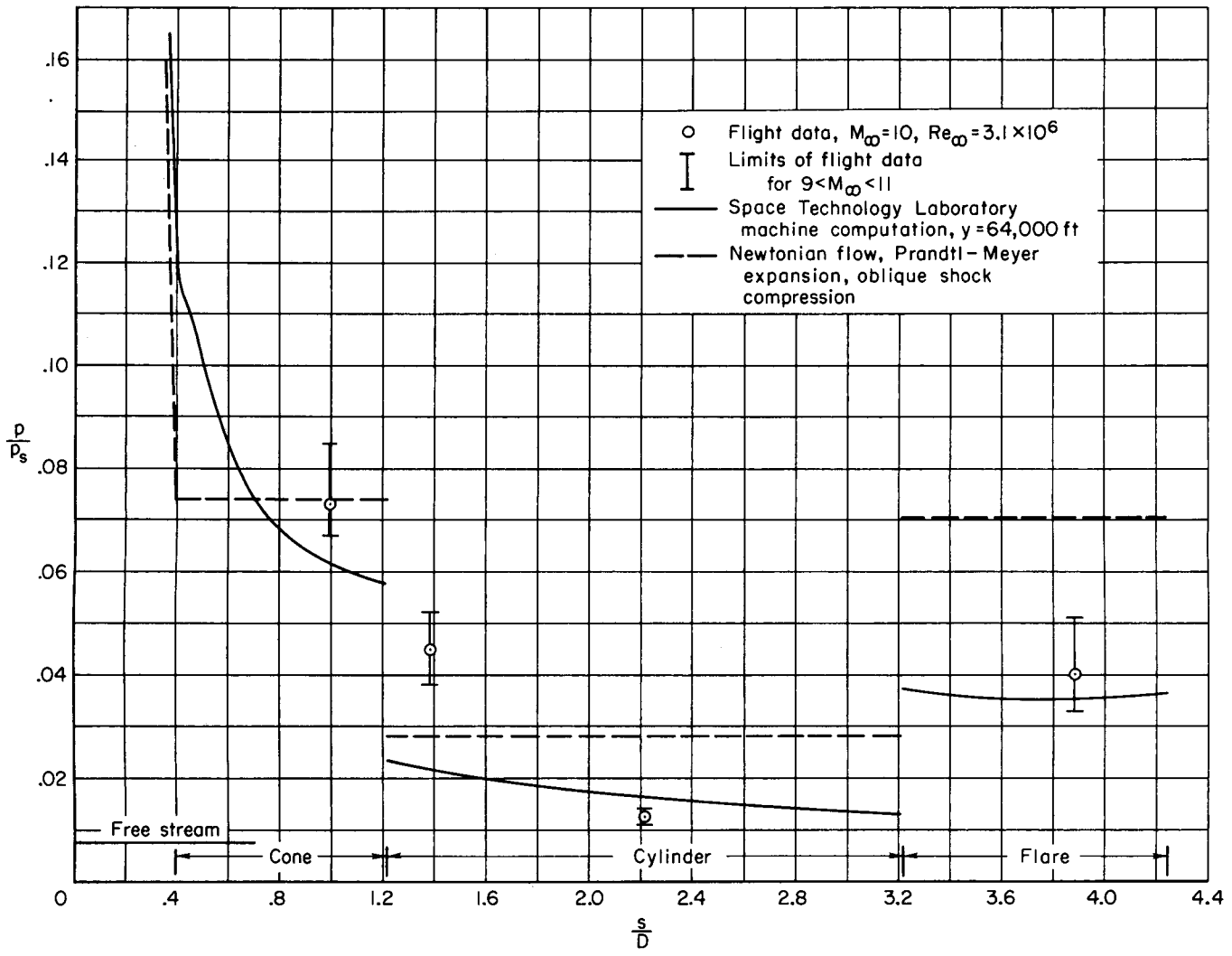

Figure 13.- Comparison of measured pressures with theoretical predictions; M_∞=10, Re_∞=3.1×10⁶.

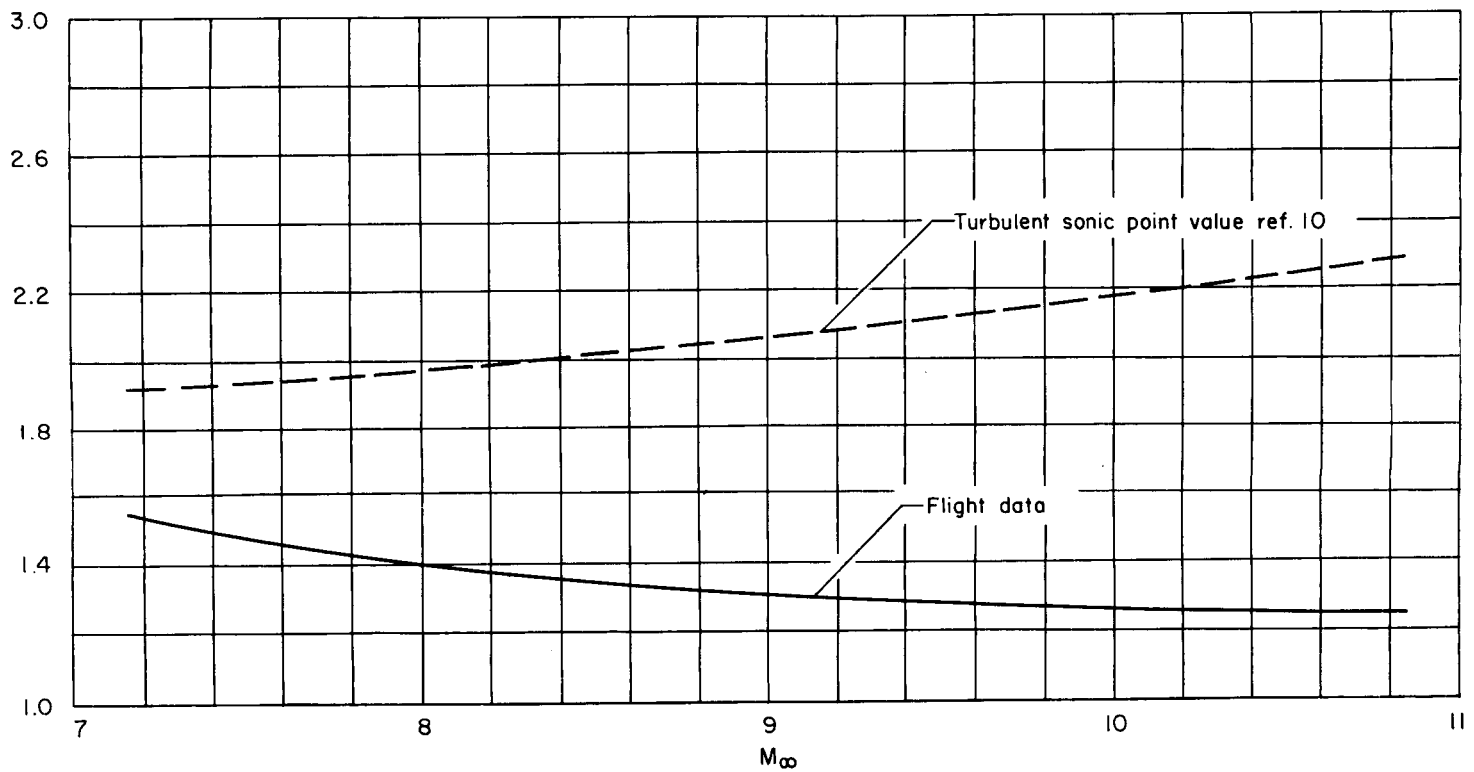

Figure 14.- Comparison with theory of heating rate at thermocouple station number 1.

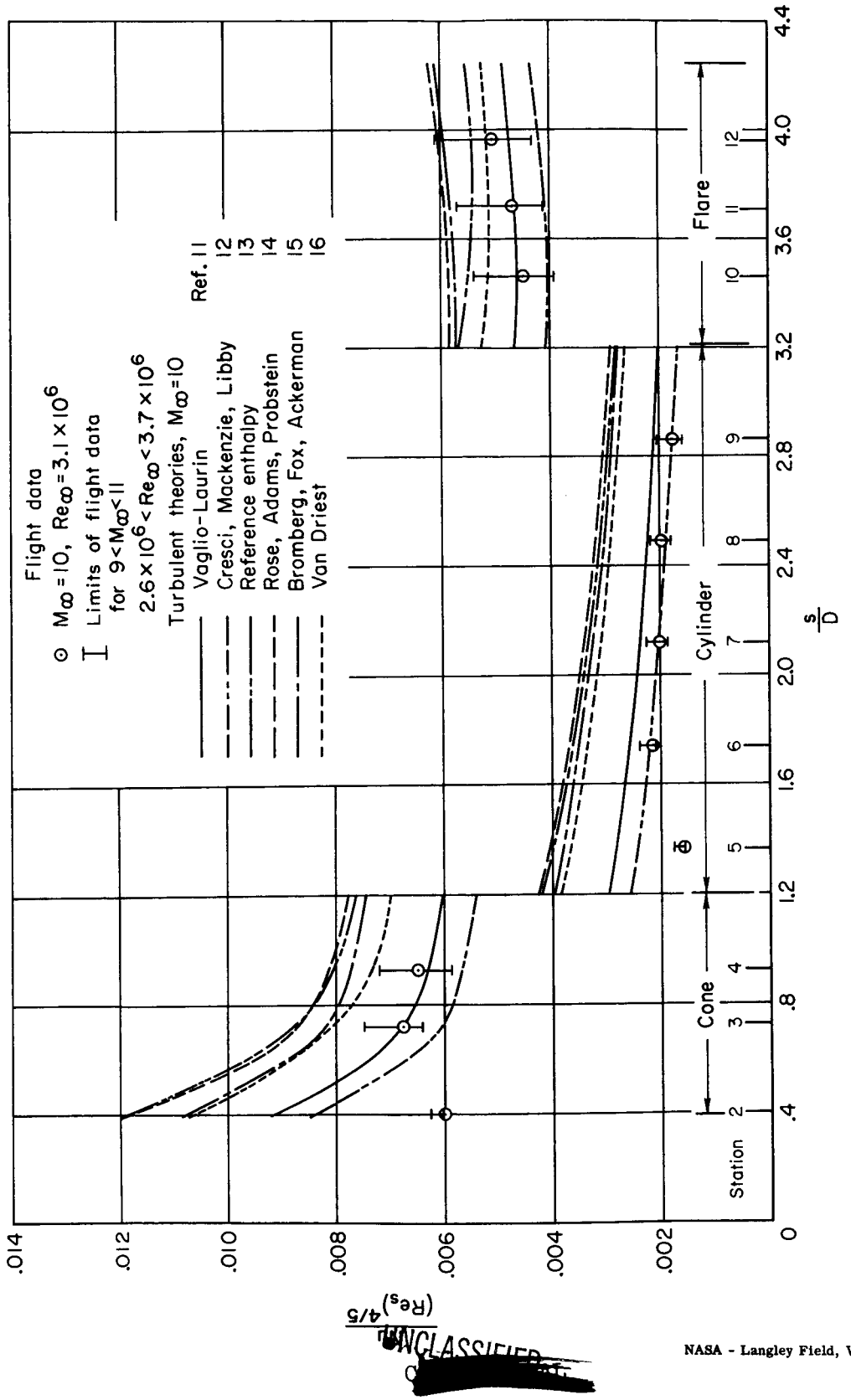

Figure 15.- Comparison of theoretical predictions with experimental heat-transfer distribution along the model.